



**HAL**  
open science

# Structural and kinematic evolution of strike-slip shear zones around and in the Central Tianshan: insights for eastward tectonic wedging in the southwest Central Asian Orogenic Belt

Zhiyuan He, Bo Wang, Xinghua Ni, Johan de Grave, Stéphane Scaillet, Yan Chen, Jiashuo Liu, Xin Zhu

## ► To cite this version:

Zhiyuan He, Bo Wang, Xinghua Ni, Johan de Grave, Stéphane Scaillet, et al.. Structural and kinematic evolution of strike-slip shear zones around and in the Central Tianshan: insights for eastward tectonic wedging in the southwest Central Asian Orogenic Belt. *Journal of Structural Geology*, 2021, 144, pp.104279. 10.1016/j.jsg.2021.104279 . insu-03105432

**HAL Id: insu-03105432**

**<https://insu.hal.science/insu-03105432>**

Submitted on 11 Jan 2021

**HAL** is a multi-disciplinary open access archive for the deposit and dissemination of scientific research documents, whether they are published or not. The documents may come from teaching and research institutions in France or abroad, or from public or private research centers.

L'archive ouverte pluridisciplinaire **HAL**, est destinée au dépôt et à la diffusion de documents scientifiques de niveau recherche, publiés ou non, émanant des établissements d'enseignement et de recherche français ou étrangers, des laboratoires publics ou privés.

# Journal Pre-proof

Structural and kinematic evolution of strike-slip shear zones around and in the Central Tianshan: insights for eastward tectonic wedging in the southwest Central Asian Orogenic Belt

Zhiyuan He, Bo Wang, Xinghua Ni, Johan De Grave, Stéphane Scaillet, Yan Chen, Jiashuo Liu, Xin Zhu

PII: S0191-8141(21)00003-1

DOI: <https://doi.org/10.1016/j.jsg.2021.104279>

Reference: SG 104279

To appear in: *Journal of Structural Geology*

Received Date: 2 September 2020

Revised Date: 29 December 2020

Accepted Date: 5 January 2021

Please cite this article as: He, Z., Wang, B., Ni, X., De Grave, J., Scaillet, S., Chen, Y., Liu, J., Zhu, X., Structural and kinematic evolution of strike-slip shear zones around and in the Central Tianshan: insights for eastward tectonic wedging in the southwest Central Asian Orogenic Belt, *Journal of Structural Geology*, <https://doi.org/10.1016/j.jsg.2021.104279>.

This is a PDF file of an article that has undergone enhancements after acceptance, such as the addition of a cover page and metadata, and formatting for readability, but it is not yet the definitive version of record. This version will undergo additional copyediting, typesetting and review before it is published in its final form, but we are providing this version to give early visibility of the article. Please note that, during the production process, errors may be discovered which could affect the content, and all legal disclaimers that apply to the journal pertain.

© 2021 Elsevier Ltd. All rights reserved.



**Credit authorship contribution statement**

**Zhiyuan He:** Conceptualization, Field Investigation, Methodology, Writing - original draft. **Bo Wang:** Conceptualization, Field Investigation, Methodology, Writing - review & editing, Supervision. **Xinghua Ni:** Field Investigation, Methodology, Writing - review & editing. **Johan De Grave:** Writing - review & editing, Co-supervision. **Stephane Scaillet:** Methodology, Writing - review & editing. **Yan Chen:** Field Investigation, Writing - review & editing. **Jiashuo Liu:** Field Investigation, Writing - review & editing. **Xin Zhu:** Methodology, Writing - review & editing.

1 **Structural and kinematic evolution of strike-slip shear zones around**  
2 **and in the Central Tianshan: insights for eastward tectonic wedging**  
3 **in the southwest Central Asian Orogenic Belt**

4

5 **Zhiyuan He<sup>1,2</sup>, Bo Wang<sup>1,3\*</sup>, Xinghua Ni<sup>1</sup>, Johan De Grave<sup>2</sup>, Stéphane Scaillet<sup>4</sup>,**  
6 **Yan Chen<sup>4</sup>, Jiashuo Liu<sup>1</sup>, Xin Zhu<sup>1</sup>**

7

8 <sup>1</sup> State Key Laboratory for Mineral Deposits Research, School of Earth Sciences and  
9 Engineering, Nanjing University, 210023 Nanjing, China

10 <sup>2</sup> Laboratory for Mineralogy and Petrology, Department of Geology, Ghent University,  
11 Krijgslaan 281 S8, 9000, Ghent, Belgium

12 <sup>3</sup> Institute of Continental Geodynamics, Nanjing University, 210023 Nanjing, China

13 <sup>4</sup> Université d'Orléans, CNRS, ISTO, UMR 7327, F-45071, Orléans, France

14

15 \*Corresponding author: Bo Wang ([bwang@nju.edu.cn](mailto:bwang@nju.edu.cn); [burh\\_cw@yahoo.com](mailto:burh_cw@yahoo.com))

16

17 **Abstract**

18 In order to better understand the late Paleozoic tectonic evolution of the  
19 southwestern Central Asian Orogenic Belt (CAOB), we carried out structural and

20 geochronological studies on the poorly investigated Xiaergou and Wulasitai shear  
21 zones around and in the Chinese Central Tianshan. The Xiaergou shear zone is the  
22 connecting segment between the North Tianshan Fault and Main Tianshan Shear Zone  
23 along the northern margin of the Yili - Central Tianshan blocks, it strikes NW-SE with  
24 a width of ~3-5 km and shows predominant dextral kinematics. Zircon U-Pb ages of  
25 pre- and syn-kinematic granitic dykes within the Xiaergou shear zone indicate that the  
26 dextral shearing was active at ~312-295 Ma. The Wulasitai shear zone is a high-strain  
27 belt occurring in the interior of the Central Tianshan block, it extends NW-SE for  
28 more than 40 km with variable widths of ~1-5 km, steep mylonitic foliations and  
29 sub-horizontal stretching lineation are well developed and various kinematic  
30 indicators suggest prevailing sinistral shearing. New biotite  $^{40}\text{Ar}/^{39}\text{Ar}$  ages of two  
31 meta-sedimentary rocks, together with the published metamorphic zircon ages  
32 constrain the timing of the sinistral shearing at ~312-301 Ma. Our new results  
33 combined with the previous studies reveal that the dextral strike-slip shear zones  
34 framing the Central Tianshan formed almost simultaneously in the latest  
35 Carboniferous (~310 Ma) and lasted until the middle to late Permian. They resulted  
36 from the eastward tectonic wedging and relative rotations between continental blocks  
37 in the SW CAOB. The sinistral shearing of the Wulasitai shear zone within the  
38 Central Tianshan was likely generated due to differential eastward motions of the  
39 northern and southern parts of the Central Tianshan.

40

41 **Keywords:** Late Paleozoic; Tianshan/Tien Shan; Intracontinental deformation;

42 Transcurrent tectonics; Oblique convergence and accretion; Block rotation

43

## 44 **1. Introduction**

45 Transcurrent tectonics generally refers to large strike-slip faulting system in  
46 which the displacement vector is parallel to the strike of fault due to plate motions on  
47 a sphere (Freund, 1974; Onstott and Hargraves, 1981; Beck, 1983; Sylvester, 1988).  
48 Transcurrent tectonics usually forms at plate boundaries by oblique plate convergence  
49 (Allen, 1965; Fossen et al., 1994; Dewey et al., 1998), and accretionary orogeny  
50 (Mann, 2007). It can also develop as a transfer zone in a rift setting or a  
51 fold-and-thrust belt (Wilson, 1965; Moore, 1979). As one important manifestation,  
52 strike-slip shear zones stand for a deep version of intracontinental transcurrent  
53 tectonics characterized by plastic deformation and a tabular to sheet-like, planar or  
54 curvilinear domains (Berthé et al., 1979; Ramsay, 1980; Fossen, 2010; Davis et al.,  
55 2011). Continental-scale strike-slip shear zones typically exhibit ductile deformation  
56 fabrics with steeply-dipping foliations (Davis et al., 1986; Tapponnier et al., 1990;  
57 Leloup et al., 1995; Cao and Neubauer, 2016; Zhang et al., 2017). As a prominent  
58 dynamic process occurring in continental crust, they delimit mechanical and  
59 rheological anomalies that tend to be reactivated or have distinct impact on structural  
60 evolution during subsequent phases of tectonism (e.g., Daly et al., 1989; Holdsworth  
61 et al., 1997; Metelkin et al., 2010; Bercovici and Ricard, 2012). Thus, understanding  
62 the structural patterns and kinematics of strike-slip shear zones as well as their

63 tectonic mechanisms is an important issue in continental dynamics research.

64 The Tianshan (Tien Shan) Orogen lies in the southernmost part of the Central  
65 Asian Orogenic Belt (CAOB), or the Altaïds, which is the largest Phanerozoic  
66 orogenic system on the world formed by progressive amalgamation of various  
67 microcontinents, island arcs, seamounts, oceanic plateaus, and accretionary  
68 complexes (Şengör et al., 1993; Jahn et al., 2000; Xiao et al., 2003; Windley et al.,  
69 2007; Wilhem et al., 2012). Following successive accretions to the northern margin of  
70 the Tarim Craton in late Paleozoic, the Tianshan Orogen and adjacent areas underwent  
71 large-scale transcurrent tectonics that greatly influenced the tectonic framework of the  
72 SW CAOB (Allen et al., 1995; Şengör and Natal'in, 1996; Laurent-Charvet et al.,  
73 2002, 2003; Wang et al., 2007a, 2009, 2014; Li et al., 2015, 2020). Therefore,  
74 recognizing the styles of transcurrent deformation is crucial for deciphering the  
75 orogenic history and tectonic transition from convergent to intracontinental evolution  
76 of this giant belt.

77 One of the most remarkable features of the Tianshan Orogen is the occurrence of  
78 two large-scale ductile shear zones that are parallel to major ophiolitic sutures (i.e. the  
79 North Tianshan Fault-Main Tianshan Shear Zone and Nalati-Baluntai Fault,  
80 respectively) (Figs. 1 and 2). Numerous studies have suggested that these two shear  
81 zones resulted from Permian regional transpressional and/or transtensional tectonics,  
82 with evidence of both general dextral strike-slip shearing and folding induced by  
83 lateral displacements (Yin and Nie, 1996; Shu et al., 1999; Laurent-Charvet et al.,  
84 2002, 2003; Y. Wang et al., 2008; Wang et al., 2009, 2014; de Jong et al., 2009;

85 Pirajno, 2010; Tang et al., 2011; Branquet et al., 2012; Cai et al., 2012). However,  
86 other authors proposed that pure shear strain related to N-S coaxial compressional  
87 tectonics was responsible for the formation of the Jueluotage shear zone (middle  
88 segment of the Main Tianshan Shear Zone) and the Baluntai Fault, based on  
89 symmetrical structures observed (Xu et al., 2003; Yang et al., 2007). Thus, there is no  
90 consensus on the mechanism and geodynamic setting of their deformation so far. In  
91 addition to these large shear zones along boundaries between major continental units,  
92 several subordinate strike-slip faults were also reported within some continental  
93 blocks, in which mylonitic rocks are widespread (e.g., Xingdi Fault, Cai et al., 2012;  
94 Hulashan Fault, Lin et al., 2013; Wulasitai shear zone, Yang et al., 2004; He et al.,  
95 2018a). However, structural data are scarce from these high-strain shear zones.  
96 Meanwhile, it is also poorly understood how they were formed and responded to the  
97 complex accretionary and collisional orogenesis, and what their structural relationship  
98 is with large transcurrent tectonics marking the boundaries of tectonic units. Further  
99 investigation is therefore needed to obtain more information on the activity of these  
100 shear zones.

101 In this study, we investigated two contiguous strike-slip shear zones, namely, the  
102 Xiaergou and Wulasitai shear zones, which hitherto have been poorly studied. The  
103 former is a connecting part between the North Tianshan Fault and the Main Tianshan  
104 Shear Zone along the northern boundary of the Yili - Central Tianshan blocks, and the  
105 latter is a subordinate shear zone inside the Central Tianshan (Fig. 2; Yang et al., 2004;  
106 He et al., 2018a). The detailed structural, kinematic and geochronological data allow

107 us to explore the possible formation mechanism of these strike-slip shear zones  
108 developed at different scales and opposite kinematic features under an overall  
109 consistent deformation regime. This study also places further constraints on the  
110 post-orogenic intracontinental evolution of the Tianshan Orogen, and provides new  
111 insights into the eastward wedging of tectonic units between the Tarim and Siberian  
112 blocks.

113

## 114 **2. Regional Geology**

### 115 ***2.1. Tectonic units in the Chinese Tianshan***

116 The Tianshan Orogen stretches east-west for about 2500 km from eastern  
117 Xinjiang in NW China to central Uzbekistan (Fig. 1). This orogenic belt was built by  
118 multi-stage subduction of the Paleo-Asian oceanic plate and the subsequent welding  
119 between the Kazakhstan-Yili block and Tarim Craton during the Paleozoic (e.g., Allen  
120 et al., 1993; Gao et al., 1998, 2009; Charvet et al., 2007, 2011; Wang et al., 2008,  
121 2011, 2018; Xiao et al., 2013), and was reactivated during the Meso-Cenozoic as a  
122 far-field response of Qiangtang-Lhasa and India-Asia collisions (e.g., Molnar and  
123 Tapponnier, 1975; Avouac et al., 1993; De Grave et al., 2007; Glorie and De Grave,  
124 2016). The Chinese segment of the Tianshan Orogen is sandwiched between the  
125 Junggar and Tarim basins (Fig. 1B). According to the differences in basement nature  
126 and tectonic settings, the Chinese Tianshan is traditionally subdivided into four  
127 tectonic units separated by regional crustal-scale faults, namely, the North Tianshan,

128 Yili Block, Central Tianshan and South Tianshan from north to south (Fig. 2; Xiao et  
129 al., 1992, 2004; Gao et al., 1998; Charvet et al., 2007).

130 The North Tianshan is an accretionary complex formed by the subduction and  
131 accretion of the Junggar - North Tianshan oceanic plate. It is composed of late  
132 Paleozoic sedimentary-volcanic sequences and magmatic intrusions, which occur in  
133 the Kazakhstan-Yili blocks to the west and around the Turpan-Hami (Tu-Ha) basin in  
134 the east. (e.g., Wang et al., 2006; Han et al., 2010; Zhang et al., 2016; Wali et al.,  
135 2018). The Yili Block represents the eastern part of the Kazakhstan microcontinent,  
136 and is a wedge-shaped area between the North and Central Tianshan blocks (Figs. 1B  
137 and 2), it consists of Meso- to Neoproterozoic basements, Paleozoic sedimentary  
138 covers and magmatic arc rocks that were generated mostly by the southward  
139 subduction of the Junggar oceanic plate (e.g., Gao et al., 1998, 2009; Hu et al., 2000;  
140 Charvet et al., 2007, 2011; Wang et al., 2007b, 2014a; Liu et al., 2014; Cao et al.,  
141 2017; Zhu et al., 2019a). Bordered by the Main Tianshan Shear Zone to the north and  
142 the Baluntai Fault to the south, the Central Tianshan refers to a ribbon-like domain  
143 extending from the Nalati Range in the west to Xingxingxia areas in the east (Fig. 2),  
144 it consists of Precambrian metamorphic basement (e.g., Hu et al., 2000; He et al.,  
145 2014, 2015, 2018b; Gao et al., 2015; X.S. Wang et al., 2017), early Paleozoic  
146 magmatic arc sequences, late Paleozoic sedimentary strata and Paleozoic intrusions  
147 (e.g., Shi et al., 2007; Dong et al., 2011; Lei et al., 2011; Ma et al., 2014; Zhong et al.,  
148 2015). The South Tianshan is confined to the region between the Nalati - Baluntai  
149 faults and the northern Tarim margin. This unit contains an early Paleozoic

150 continental arc and late Paleozoic sedimentary cover, which were formed during the  
151 successive closure of the South Tianshan Ocean and several back-arc basins (e.g., Gao  
152 et al., 1998, 2009; Wang et al., 2010, 2011, 2018; Jiang et al., 2014; Alexeiev et al.,  
153 2015; Han et al., 2016; Zhong et al., 2017, 2019).

154

## 155 ***2.2. Large-scale shear zones in the Chinese Tianshan***

156 The main tectonic units described above contact with each other by large-scale  
157 shear zones that extends roughly east-west and are sub-parallel to the ophiolitic  
158 mélange zones developed along the Bayingou - Mishigou - Gangou and Atbashi -  
159 Kekesu - Wuwamen areas (Figs. 1 and 2; Wang et al., 2008; Charvet et al., 2011).

160 The Main Tianshan Shear Zone (MTSZ) (Shu et al., 1999; Laurent-Charvet et al.,  
161 2002; Liu et al., 2020) is the tectonic boundary between the North Tianshan and  
162 Central Tianshan and it stretches for over 700 km from Xiaergou-Gangou eastward to  
163 Weiya (Fig. 1B) (XIGMR, 2007). Along this shear zone, Precambrian schists and  
164 gneisses, Paleozoic granitoids and volcanics, as well as ophiolitic rocks were  
165 mylonitized and they generally exhibit sub-vertical mylonitic foliations with  
166 sub-horizontal stretching lineation (Shu et al., 1999, 2002; Laurent-Charvet et al.,  
167 2002, 2003; Li et al., 2020). Consistent asymmetric fabrics indicate a right-lateral  
168 strike-slip movement, with thrusting and/or normal faulting components, probably  
169 formed in transpressional and/or transtensional settings (Laurent-Charvet et al., 2003;  
170 Wang et al., 2008; Yang et al., 2009; Li et al., 2020; Liu et al., 2020). The North

171 Tianshan Fault (NTF) is essentially the westward continuation of the MTSZ and it  
172 runs into Kazakhstan, separating the Yili block to the south from the Chinese North  
173 Tianshan to the north (Fig. 2). Kinematic features along the NTF also indicate a  
174 dextral ductile shearing (Zhou et al., 2001; Wang et al., 2006, 2009; de Jong et al.,  
175 2009; Yang et al., 2009; Zhu, 2011; Liu et al., 2020).

176 The Nalati Fault (NF) occurs along the Haerke-Nalati ranges in the South  
177 Tianshan (Fig. 1B), and is a large ductile shear zone ~5-15 km wide (e.g., Wang et al.,  
178 2010; Charvet et al., 2011; Han et al., 2011). It continues eastwards to merge with the  
179 NTF near the Bingdaban area (Figs. 1B and 2). This ductile shear zone was active  
180 mainly in the Permian and reworked the Carboniferous suture zone (Akeyazi-Kekesu  
181 ophiolite mélanges and high-pressure metamorphic belt) (Fig. 1B) formed by the  
182 subduction of the South Tianshan oceanic plate (e.g., Gao et al., 1998, 2009; Lin et al.,  
183 2009; Qian et al., 2009; Wang et al., 2009, 2010; Long et al., 2011; Xu et al., 2013;  
184 Zhong et al., 2017, 2019). Diverse mylonites, foliated meta-sedimentary rocks and  
185 gneissic granitoids are well exposed in this shear zone, and structural studies from the  
186 Kekesu high-pressure metamorphic belt and north of Bayinbulak (Fig. 1B) indicate  
187 dextral kinematics (XBGMR, 1993; Li and Liu, 1997; Wang et al., 2007c, 2010; Lin  
188 et al., 2009; Zhong et al., 2019).

189 The Baluntai Fault (BF) stands for the boundary between the Central Tianshan to  
190 the northeast and the South Tianshan to the southwest (Alexeiev et al., 2015; Wang et  
191 al., 2018; Zhong et al., 2019). It extends from the north of Bayinbulak, nearly parallel  
192 to the NTF - MTSZ, to the Sangshuyuanzi area to the east (Figs. 1B and 2) (XIGMR,

193 2007). Foliated schists and gneisses, mylonitic rocks and ductilely deformed  
194 granitoids are widely distributed along the BF, which also partially reworked the  
195 Wuwamen - Guluogou ophiolite mélanges (Fig. 2) (XBGMR, 1993, Yang et al., 2004;  
196 Deng et al., 2006; M. Wang et al., 2014; Wang et al., 2018). Localized coaxial pure  
197 strain was described in the south of Baluntai regions and was considered as the result  
198 of N-S compression (Yang et al., 2007); however, most structural investigations from  
199 the Sangshuyuanzi, Baluntai areas and their eastward continuation demonstrated  
200 dextral strike-slip shearing (Laurent-Charvet et al., 2003; Y. Wang et al., 2008; Wang  
201 et al., 2009; Xu et al., 2011; Cai et al., 2012; Zhong et al., 2015; Li et al., 2020).

202

### 203 **3. Overall geometry, structures and kinematics of the Xiaergou and** 204 **Wulasitai shear zones**

205 Our structural investigations were conducted along several sections crossing the  
206 Xiaergou and Wulasitai shear zones around and within the Central Tianshan (Figs.  
207 2-10). In the following sections, we present the main lithological units in the two  
208 shear zones and their structural and kinematic features.

209

#### 210 ***3.1. Xiaergou Shear Zone***

211 As the eastern part of the NTF, the Xiaergou Shear Zone (XSZ) is a ~NW-SE  
212 trending mylonitic belt with a width of ~3-5 km, and was locally reworked or

213 truncated by brittle reverse and/or left-lateral strike-slip faults (Figs. 2 and 3). Due to  
214 difficult physical conditions our field observations were limited to a 5-km-long  
215 section mainly along its strike near the Xiaergou village (Figs. 3B and 4).

216

### 217 *3.1.1. Lithological units*

218 Silurian to Devonian marine sequences were affected by the ductile deformation  
219 along the XSZ. Silurian meta-sediments belong to the middle Ahebulake Group and  
220 consist of marbles, greywackes, schists, phyllites and calcareous sandstones with  
221 interlayered tuff. Devonian sequences are represented by the middle Tiangeer Group  
222 that is dominated by basaltic tuffs, tuffaceous sandstones and marbles (XBGMR,  
223 1993). Both groups are in contact with each other along a steep N-dipping reverse  
224 fault (Figs. 3 and 4).

225 Early Paleozoic granodiorites and late Paleozoic granites are well exposed  
226 within and across the shear zone (Figs. 3B and 4). The late Paleozoic granites were  
227 dated at ~370-337 Ma (zircon U-Pb ages) and were interpreted to be related to the  
228 subduction of the North Tianshan oceanic plate and the collision between the Central  
229 and North Tianshan (including Tu-Ha basin) during the early Carboniferous (Ma et al.,  
230 2014; Yin et al., 2017). In addition, numerous undeformed granitic and diabase dykes  
231 of unknown ages intruded into Silurian-Devonian meta-sedimentary and volcanic  
232 rocks as well as the Paleozoic plutons (Figs. 3 and 4).

233

234 *3.1.2. Structures and kinematics*

235 Except for the undeformed granitic and diabase dykes intruding the XSZ, all  
236 other lithological units mentioned above underwent intensive ductile shearing,  
237 showing well-defined ~E-W or ~ENE-WSW-striking steep ( $40^\circ$  to  $78^\circ$ ) mylonitic  
238 foliations (S1) associated with pervasive stretching lineation (L1) gently plunging  
239 ( $<40^\circ$ ) to E/NE or W/SW (Figs. 4A-B and 5A-D). Both the strikes of S1 foliations  
240 and the plunges of L1 lineation are sub-parallel to the overall strike of the shear zone.  
241 The mylonitic foliations and stretching lineation are usually defined by elongated  
242 quartz and feldspar ribbons and mica aggregates (Figs. 5 and 6). In the  
243 Silurian-Devonian metasedimentary rocks, the S1 is predominantly dipping to the  
244 ~N-NNE with variable dip angles ranging from  $42^\circ$  to  $76^\circ$ , and is parallel to the  
245 locally preserved S0 bedding planes (Fig. 4A-B). The K-feldspar porphyroclasts are  
246 elongated and oriented parallel to the shearing foliations. In addition, mylonitic felsic  
247 dykes intruding the marbles and schists also exhibit steep foliations and  
248 sub-horizontal mineral stretching lineation, which are defined by a preferred  
249 orientation of elongated feldspar and quartz grains (Figs. 4C and 5D). Leuco-granitic  
250 dykes and their host granitic pluton both display ~NE-SW-striking mylonitic  
251 foliations with ~ENE/WSW plunging lineation (Figs. 4A-B and 5A), which are  
252 oblique to the general strike of the shear zone, probably due to localized rotation  
253 related to the NE-striking brittle reverse fault (Fig. 4A).

254 Disjunctive cleavage in granodiorites shows a general strike of  $160^\circ$ , sub-parallel  
255 to the shear zone; and shear bands suggest a dextral sense of shearing (Fig. 5E). In

256 highly deformed marbles, sheath folds and A-type folds were well preserved, whose  
257 hinges are parallel to the stretching lineation; on the X-Z plane (perpendicular to  
258 foliation and parallel to lineation), the asymmetric fold shapes present a dextral  
259 shearing (Fig. 5F). S-C fabrics can be recognized in marbles as well, the S-foliation is  
260 represented by elongated calcite veins, and a dextral sense of movement is also  
261 indicated (Fig. 5G). It is worth noting that sinistral shearing was also occasionally  
262 preserved, as revealed by asymmetric quartz lens in a small-scale greenschist outcrop  
263 (Fig. 5H). Under microscope, mylonitic granitoids and tuffaceous sandstones contain  
264 plenty of kinematic indicators, such as S-C fabrics, feldspar bookshelf texture,  
265 sigmoid asymmetric feldspar porphyroclasts and mica pressure shadows showing a  
266 principal dextral sense of shearing (Fig. 6A-D), sinistral kinematics was only locally  
267 developed and is associated with dextral kinematics (Fig. 6E-F).

268

### 269 **3.2. Wulasitai Shear Zone**

270 The Wulasitai shear zone (WSZ) is a remarkable subordinate high-strain  
271 deformation zone occurring within the Central Tianshan, it extends NW-SE, nearly  
272 parallel to the NTF and BF, for more than 40 km with variable widths of ~1-5 km  
273 (Figs. 2 and 7). This high-strain mylonitic belt merged westwards into the NF, and it is  
274 covered eastwards by strongly weathered granites, vegetation and glacier (Fig. 2), it is  
275 possible that the WSZ connects the MTSZ in the Yuergou area (XIGMR, 2007).

276

277 *3.2.1. Lithological units*

278 A variety of rocks are well exposed along the WSZ and were significantly  
279 deformed by ductile shearing, they mainly include Proterozoic paragneiss, early  
280 Paleozoic sedimentary rocks and granodiorites, and late Paleozoic granites (Fig. 7B;  
281 XBGMR, 1993).

282 Proterozoic paragneiss occur north of the Wulasitai village (Fig. 7B) and were  
283 previously assigned to the Paleoproterozoic Xingxingxia Group (XBGMR, 1993;  
284 XIGMR, 2007). However, recent zircon U-Pb dating indicated that some of these  
285 meta-sedimentary rocks were likely deposited in the early Devonian to late  
286 Carboniferous (Shu et al., 2013; Wang et al., 2018). Early Paleozoic  
287 meta-sedimentary rocks dominantly comprise paragneiss, marbles, greenschists,  
288 deformed quartz sandstones and greywackes, they were considered as Silurian in age,  
289 but some of them were recently constrained as Devonian (He et al., 2018a).

290 Paleozoic plutonic rocks along the WSZ include early Paleozoic granodiorites  
291 and late Paleozoic granites intruding the “Proterozoic” and “Silurian”  
292 meta-sedimentary rocks (Fig. 7B). Migmatites are frequently associated with the  
293 granodiorites and can also be observed in the meta-sandstones. Some late Paleozoic  
294 granites exposed along the WSZ were dated at ~354-332 Ma (He et al., 2018a).

295 These ductilely deformed and metamorphosed sedimentary rocks are  
296 unconformably covered by undeformed and gently tilted Jurassic sandstones (Fig.  
297 7B).

298

299 *3.2.2. Structures and kinematics*

300 Along the WSZ, ~E-W or ~NW-SE-striking, diversely S/SW- or N/NE-dipping  
301 mylonitic foliations (S1) and associated mineral stretching lineation (L1) are well  
302 developed in most lithological units (Figs. 8 and 9A-E). The dip angles of foliations  
303 vary from 30° to 80°, and the plunging angles of lineation are 3°-40° (Fig. 8). In  
304 general, the steeper foliations bearing shallower lineation occur along the straight  
305 segment, and gentle foliations with nearly down-dip lineation are mostly observed at  
306 the turning segment of the WSZ (Figs. 7 and 8). Silurian meta-greywackes underwent  
307 intensive ductile deformation displaying steep mylonitic foliations and gentle  
308 stretching lineation (Fig. 9A). Some paragneiss and phyllites show gently  
309 south-dipping foliations and sub-horizontal stretching lineation defined by elongated  
310 ribbons of felsic melts, and coeval sub-S-N crenulation cleavages (L1') represented  
311 by hinges of microfolds full of mica and sericite (Fig. 9B-C). In migmatites,  
312 foliation-parallel leucocratic veins reflect a low-degree partial melting, elongated  
313 K-feldspar and quartz ribbons in the leucosome indicate a syn-kinematic transport of  
314 melts (Fig. 9B). The granitic rocks were also ductilely deformed showing mylonitic  
315 foliations and ~E-W-trending stretching lineation characterized by elongated feldspar  
316 and quartz ribbons and oriented micas (Fig. 9D-E).

317 Overall bending geometry suggests that localized transpressional deformation  
318 affected the WSZ. For example, along a ~NE-SW profile across the bending segment

319 of the WSZ, folded and duplicated quartz veins occur in mylonitic granites with the  
320 axial planes parallel to the S1 foliation, asymmetric folds and shear bands indicate a  
321 top-to-the-southwest shearing (Fig. 9F). Moreover, strike-slip motions along the WSZ  
322 were well recorded by a series of apparent kinematic indicators. At the field scale,  
323 asymmetric intrafolial microfolds in the meta-rhyolites (Fig. 9G), shear bands in the  
324 meta-sandstones (Fig. 9H), and fractured and offset felsic veins in the mylonitic  
325 granites (Fig. 9I) suggest a sinistral shearing along the strike of the shear zone. In  
326 addition, microscopic textures such as the sigmoid biotite mica fishes (Fig. 10A),  
327 shear bands and pressure shadows composed of mica around K-feldspar  
328 porphyroclasts (Fig. 10B-C), S-C fabrics and  $\sigma$ -type feldspar porphyroclasts (Fig.  
329 10D-E) consistently demonstrate a sinistral sense of shear. However, dextral motion is  
330 also indicated by sigmoid quartz and feldspar porphyroclasts (Fig. 10F) that are  
331 occasionally visible in few samples showing predominantly sinistral shearing.

332

#### 333 **4. Temperature conditions of the ductile deformation**

334 Quartz is one of the most sensitive minerals during plastic deformation. In a  
335 shear zone, quartz can be deformed via different mechanisms under various  
336 temperature conditions. Previous studies established relationships between  
337 deformation mechanisms and physical conditions based on naturally and  
338 experimentally deformed rocks, e.g., types of quartz dynamic recrystallization and  
339 corresponding temperatures, are widely applied in studies of shear zones (e.g., Hirth

340 et al., 2001; Stipp et al., 2002a, 2002b; Passchier and Trouw, 2005; Law, 2014). Here  
341 we estimated deformation temperatures of these two shear zones according to the  
342 criteria for quartz dynamic recrystallization proposed by Stipp et al. (2002a). The  
343 studied samples were collected from the axial parts of the shear zones (Figs. 4 and 8)  
344 so that they may reflect the peak conditions of ductile shearing. In order to avoid  
345 possible large uncertainty brought by the sampling effect, at least two samples were  
346 taken from each sampling site for thin section observation. Detailed microstructural  
347 descriptions and temperature estimations are given in supplementary Table S1.

348 Our observations suggest that the sub-grain rotation is the dominant mechanism  
349 of quartz dynamic recrystallization in both the XSZ and WSZ (Fig. 11; Table S1). In a  
350 number of samples, numerous new small grains produced by both bulging and  
351 sub-grain rotation mechanisms occur around the original quartz grains, revealing a  
352 typical core-mantle structure (Fig. 11A, B and D), and the elongated quartz ribbons  
353 parallel to main foliations reflect intensive dislocation creep deformation (Fig. 11C, E  
354 and F). Grain boundary migration recrystallization appears more frequently in the  
355 XSZ (Fig. 11C), indicating a higher temperature condition compared to the WSZ.  
356 Generally, deformation temperatures in the XSZ are estimated as ~460-510 °C,  
357 slightly higher than the temperature conditions of the WSZ (~450-485 °C) (Fig. 12;  
358 Table S1). In addition, feldspar only displays bulging recrystallization and no clear  
359 evidence for sub-grain rotation was identified in both shear zones, suggesting a  
360 maximum temperature threshold of ~550-600 °C for ductile shearing. It is noted that  
361 the estimated temperatures here only refer to the pervasive dextral shearing of the

362 XSZ and sinistral shearing of the WSZ. Meanwhile, sinistral kinematics within the  
363 XSZ and dextral kinematics along the WSZ are only locally preserved as described  
364 before, their corresponding deformation temperatures are thus difficult to be  
365 determined without efficient indicators.

366

## 367 **5. Geochronology**

368 In order to constrain the timing of ductile deformation, new isotopic data were  
369 obtained by zircon LA-ICP-MS U-Pb and biotite  $^{40}\text{Ar}/^{39}\text{Ar}$  dating. Sample locations  
370 are marked on Figs. 4 and 8, analytical procedures are described in Appendix, and  
371 analytical data are provided in supplementary Tables S2 and S3.

372

### 373 *5.1. Zircon U-Pb ages for pre- and syn-kinematic granitic dykes in the Xiaergou*

#### 374 *Shear Zone*

375 Pre- and syn-kinematic plutons develop along the XSZ. The syn-kinematic ones  
376 were emplaced during the ductile shearing, some occur as migmatitic veins due to in  
377 situ partial melting of the host rocks and some injected from deep-seated magma via  
378 foliations or faults (Hutton, 1988; Pitcher, 1997; Pirajno, 2010; Wang et al., 2014b).  
379 One distinct character of syn-kinematic dykes is that their distributions are only  
380 limited within the shear zone. This situation differs from that of the pre-kinematic  
381 dykes, which are distributed not only within but also outside the shear zone and they

382 usually crosscut the shear zone or lithological boundaries (Searle, 2006; Rolland et al.,  
383 2009; Cao et al., 2011; J. Liu et al., 2020). From the XSZ, one sample of  
384 pre-kinematic granite dyke and another of syn-kinematic dyke intruding the Silurian  
385 marbles and late Paleozoic granites (~370-337 Ma; Ma et al., 2014; Yin et al., 2017)  
386 (Fig. 4), were dated using the zircon LA-ICP-MS U-Pb method.

387 Sample 44-B was taken from a granitic dyke of ~1m wide (Fig. 13A), which  
388 displays sharp contact with the host rocks. Both the dyke and its host rocks show  
389 similar deformation fabrics, i.e., steeply N-dipping mylonitic foliations and shallowly  
390 plunging lineation, indicating a strike-slip shearing, and a pre-kinematic emplacement  
391 of the granite dyke. The sample mainly contains K-feldspar and quartz with minor  
392 biotite and muscovite (Fig. 13B). The zircon grains from this sample are commonly  
393 euhedral and 100-150  $\mu\text{m}$  in length, their CL (Cathodoluminescence) images  
394 generally show well-developed concentric oscillatory zoning (Fig. 13C). A total of  
395 fifteen analyses were carried out on twelve zircons, showing Th/U ratios of 0.4-0.8  
396 (Table S2), indicating a magmatic origin according to the descriptions of Corfu et al.  
397 (2003). Therein, 12 out of 15 analyses yielded a concordant age of  $311.9 \pm 2.4$  Ma  
398 (MSWD = 0.21; Fig. 13D), including two analyses on the modified rims (Nos. 1 and  
399 14; Fig. 13C), while the unmodified parts of these two zircons yielded older  
400  $^{206}\text{Pb}/^{238}\text{U}$  ages of ~342 Ma and ~331 Ma (Fig. 13D), comparable to the ages of the  
401 host granites, from which these two zircons were likely derived. One additional zircon  
402 yielded much older age of ~431 Ma, and it is probably inherited.

403 Sample 49-C was collected from another granitic dyke intruding the Silurian

404 marbles and tuffaceous sandstones (Fig. 4). The dyke is ~1-1.5 m wide and shows  
405 boudinage structure and well-developed mylonitic foliations and stretching lineation  
406 (Fig. 13E), consistent with those of the host rocks. Generally parallel contact between  
407 the dyke and its host rocks to the main mylonitic foliations, and high-strain  
408 superplastic creep of quartz (Fig. 13F), i.e., high-temperature syn-magmatic  
409 deformation, indicate a syn-kinematic emplacement of the dyke. The sample is  
410 fine-grained and consists of feldspar, quartz and fine-grained muscovite (Fig. 13F).  
411 Subhedral zircon crystals from this sample have length/width ratios of 2.5:1-1:1 with  
412 variable long axes of 50-200  $\mu\text{m}$  (Fig. 13G). Sixteen zircons were dated, concordant  
413 and consistent results were obtained from nine zircons with typical oscillatory zoning,  
414 indicative of an igneous origin together with their relatively high Th/U ratios  
415 (0.14-1.25) (Fig. 13G; Table S2); these nine analyses yielded a weighted mean  
416  $^{206}\text{Pb}/^{238}\text{U}$  age of  $294.6 \pm 3.7$  Ma (MSWD = 1.6; Fig. 13H), which is interpreted to  
417 represent the crystallization age of this syn-kinematic dyke. Five zircon grains yielded  
418 older ages ranging from ~332 Ma to ~1476 Ma, indicating derivation from older  
419 crustal rocks. Two additional analyses show high degrees of discordance (>10%) (Nos.  
420 12 and 15; Table S2) of which the meaning is still unclear.

421

## 422 ***5.2. Biotite $^{40}\text{Ar}/^{39}\text{Ar}$ ages for meta-sedimentary rocks in the Wulasitai Shear Zone***

423 Biotite  $^{40}\text{Ar}/^{39}\text{Ar}$  dating was performed on two samples from meta-sedimentary  
424 rocks of the Silurian Ahebulake Group in the WSZ, both samples were collected from

425 the axial part of the shear zone (Fig. 8B) and were subjected to intensive ductile  
426 shearing. Sample 01-B is a paragneiss and mainly composed of quartz, feldspar and  
427 biotite (Fig. 14A). Preferred orientation of biotite assemblages and quartz ribbons  
428 define foliations and lineation, and quartz shows undulose extinction and sub-grain  
429 rotation dynamic recrystallization (Fig. 14A). Sample 02-B is a meta-sandstone  
430 mainly containing quartz, plagioclase, K-feldspar and biotite (Fig. 14B). Despite  
431 sporadic distribution, elongation of fine-grained biotites assigned along the main  
432 foliations and lineation and filled in between the granular quartz and feldspar grains,  
433 which also show undulose extinction, bulging dynamic recrystallization, and  
434 sometimes grain boundary migration recrystallization or even probable superplastic  
435 creep as indicated by equidimensional quartz grains with relatively straight grain  
436 boundaries (Fig. 14B). Overall oblique orientation and sigmoidal shape of biotite  
437 aggregates indicate a sinistral sense of shearing (Fig. 14A-B).

438 The  $^{40}\text{Ar}/^{39}\text{Ar}$  dating results of biotites from the meta-sedimentary rocks are  
439 plotted in Fig. 14C-F, all ages are laser step-heating ages, and errors are quoted at the  
440  $1\sigma$  level. The age spectrum of biotite sample 01-B of a paragneiss are somewhat  
441 scattered, without a clear trend through the degassing steps. Apart from the initial  
442 steps, the other analyses yielded apparent ages ranging from 295 to 306 Ma (Table  
443 S3), a Total-Gas Age (TGA) of  $300.3 \pm 2.5$  Ma and a weighted mean age (WMA) of  
444  $300.5 \pm 1.6$  (MSWD = 3.7; 98% of  $^{39}\text{Ar}_K$  released) are calculated (Fig. 14C). For the  
445 biotite sample 02-B from a meta-sandstone, most analyses yielded generally  
446 consistent apparent ages (298-310 Ma) except one step that shows a much younger

447 apparent age probably due to extremely low  $^{39}\text{Ar}$  released (Table S3). The TGA and  
448 WMA of this sample are calculated at  $303.0 \pm 2.5$  Ma and  $303.4 \pm 1.3$  Ma (MSWD =  
449 1.7;  $\sim 100\%$  of  $^{39}\text{Ar}_K$ ), respectively (Fig. 14D).

450

## 451 **6. Discussion**

### 452 *6.1. Kinematic significance of the Xiaergou and Wulasitai shear zones*

453 According to the general geometry of the Xiaergou shear zone (XSZ), this  
454 structure forms the connecting segment between the North Tianshan Fault (NTF) and  
455 Main Tianshan Shear Zone (MTSZ) (Figs. 1 and 2). Based on our structural  
456 observations and kinematic analysis of prevalent macro- and micro-kinematic  
457 characteristics, the XSZ is dominated by a simple dextral shearing. This is in  
458 agreement with previous investigations along both the NTF and MTSZ (Shu et al.,  
459 1999; Laurent-Charvet et al., 2002, 2003; Wang et al., 2006, 2009; de Jong et al.,  
460 2009; Li et al., 2020). At the same time, sinistral shearing is only locally recognized  
461 along the XSZ. In the field, it only occurs in the greenschist from one observation site  
462 (Fig. 5H); in a few thin sections (samples 45-A and 52-B; Table S1), it was locally  
463 preserved along with the dominant dextral kinematics (Fig. 6E-F).

464 The Wulasitai shear zone (WSZ) was previously reported by Yang et al. (2004)  
465 near the Wulasitai village, and He et al. (2018a) traced this shear zone far westward  
466 and proposed that it can separate the Central Tianshan into northern and southern  
467 parts (Fig. 2). Based on our field and microscopic investigations, the WSZ

468 geometrically is a bending strike-slip shear zone and is kinematically dominated by  
469 sinistral shearing (Figs. 7B and 8), meanwhile, very limited dextral shearing can be  
470 distinguished in thin section (sample 06-B; Table S1) to be associated with the  
471 dominant sinistral kinematics (Fig. 10). In addition, at the bends and stepovers of the  
472 WSZ, a component of top-to-the-southwest shearing is also associated with the  
473 general sinistral shearing (Fig. 9F), and most likely resulted from strain partitioning  
474 due to transpression at the stepovers along the bending WSZ (Fig. 7), as commonly  
475 recognized in most bending strike-slip shear zones (e.g., Cunningham and Mann,  
476 2007).

477 Therefore, both the XSZ and WSZ are characterized by a co-existence of  
478 opposite kinematic features. Four possibilities might potentially explain  
479 co-occurrence of these opposite kinematics within an identical shear zone: (1) strain  
480 localization along shear zone, (2) strain partitioning between conjugate structures, (3)  
481 low differential stress or coaxial shortening perpendicular to the shear zone, or (4)  
482 multi-stage simple shear events with rotated shortening directions. Localized NE-SW,  
483 NNW-SSE and N-S sinistral shearing was previously documented along the dextral  
484 MTSZ, and was interpreted as a subordinate left-lateral shear zone conjugated with  
485 the major WNW-ESE right-lateral shearing resulted from NNW-SSE bulk shortening  
486 (Laurent-Charvet et al., 2002, 2003). In addition, sinistral ductile shearing was also  
487 reported along the Baluntai Fault (or Southern Central Tianshan Fault) and considered  
488 as the result of clockwise rotation of Tarim with respect to Central Tianshan (Deng et  
489 al., 2006) or resulting from Devonian oblique convergence (Li et al., 2020). Some

490 authors also proposed that the ductile shearing along the Central and North Tianshan  
491 formed under coaxial pure shear related to the NE-SW contraction induced by  
492 convergence between the Tarim and Central Tianshan blocks (e.g., Xu et al., 2003;  
493 Yang et al., 2007).

494 In the cases of the XSZ and WSZ, strain partitioning mostly occurred along the  
495 bending segment of the WSZ as the top-to-the-SW shearing and changes of shear  
496 directions can be observed there (Figs. 7, 9 and 10F). Shear directions also  
497 dramatically change in the XSZ but only in the overlapping segments between the  
498 overall NW-SE-striking ductile shear zone and the NE-SW-trending brittle strike-slip  
499 reverse faults (Fig. 4A). The latter cut across lithological boundaries and the mylonitic  
500 foliations of the shear zone, without any associated ductile deformation. They are not  
501 conjugate (subordinate) shear zones coeval to the NW-SE main shear zone, but rather  
502 posterior brittle faults. Local rotation related to these brittle reverse faults could be  
503 partially responsible for the changes of shear directions along the XSZ shear zone.  
504 Even though, strain partitioning and strain localization are unlikely the reasons for the  
505 opposite kinematics in the XSZ and WSZ because kinematic senses remain consistent  
506 when the shear directions (foliations) change.

507 In addition, the general sub-E-W stretching lineation and consistently low  
508 plunging (Figs. 4 and 8) in both the XSZ and WSZ indicate simple shear instead of  
509 pure shear or dominant coaxial contraction. Slight variations in lineation plunging  
510 directions and angles are the effects of bending of the shear zone and localized strain  
511 partitioning for the case of the WSZ, and the influence of localized fabrics rotation

512 related to later reworking by reverse faults for the XSZ. Moreover, development of  
513 sheath folds and A-type folds in the XSZ (Fig. 5) and syn-kinematic granites in the  
514 WSZ (Fig. 9) also indicate quite high strain rate in both shear zones, and the  
515 possibility of low differential stress can be ruled out.

516 Considering that sinistral shearing is very locally preserved in the overwhelming  
517 dextral kinematics of the XSZ, and that locally recognized dextral shearing is  
518 observed only in a sample with predominant sinistral motions from the WSZ, it is  
519 most likely that these opposite kinematics in both shear zones formed in different  
520 stages of ductile deformation. In a multi-stage deformation belt like the Tianshan  
521 Orogen, the most pervasive structures should be the result of the most intensive and  
522 younger deformation events, and the fabrics formed in earlier deformation stage(s)  
523 could be rarely preserved due to later strong overprinting and replacement. Thus, it is  
524 reasonable to suggest that the occasionally observed sinistral kinematics in the XSZ  
525 and dextral kinematics in the WSZ might represent locally preserved fabrics of earlier  
526 deformation events. However, how and when these possible earlier structures were  
527 formed is still not clear, and localized development of coeval but opposite kinematics  
528 could not be completely excluded, thus, further investigations are needed in future.

529

## 530 ***6.2. Timing of strike-slip ductile shearing around and in the Central Tianshan***

531 Along the MTSZ, the northern boundary of the Central Tianshan, mica  $^{40}\text{Ar}/^{39}\text{Ar}$   
532 ages of 290-242 Ma were obtained from the Gangou, Mishigou and Hongyuntan areas

533 (Shu et al., 2002; Laurent-Charvet et al., 2003; Cai et al., 2012), together with a  
534 muscovite  $^{40}\text{Ar}/^{39}\text{Ar}$  plateau age of  $309.7 \pm 2.2$  Ma for a mylonite from Mishigou (Xu  
535 et al., 2011), it is suggested the dextral shearing along the MTSZ occurred during the  
536 late Carboniferous to Early Triassic. Along the NTF, the westward continuation of the  
537 MTSZ, the age of dextral ductile shearing was constrained between  $\sim 270$  and  $\sim 245$   
538 Ma by mica  $^{40}\text{Ar}/^{39}\text{Ar}$  dating on mylonitic slates and foliated granites in the Du-Ku  
539 and Bingdaban areas (Laurent-Charvet et al., 2003; de Jong et al., 2009; Yang et al.,  
540 2009).

541 In this study, pre- and syn-kinematic granitic dykes in the XSZ yielded zircon  
542 U-Pb ages of  $311.9 \pm 2.4$  Ma (Fig. 13D) and  $294.6 \pm 3.7$  Ma (Fig. 13H),  
543 approximately overlapping the oldest mica  $^{40}\text{Ar}/^{39}\text{Ar}$  ages from the MTSZ and NTF.  
544 Taking into account that (1) igneous origins of the dated concordant zircons and both  
545 pre- and syn-kinematic features of the granite dykes, and (2) the estimated  
546 deformation temperatures ( $450\text{-}550$  °C) are lower than crystallization temperature of  
547 igneous zircons and closure temperature of zircon U-Pb system ( $>700$  °C; Cherniak  
548 and Watson, 2003), but higher than the closure temperatures of biotite and muscovite  
549 argon system ( $365 \pm 35$  to  $425 \pm 70$  °C; Harrison et al., 1985, 2009; McDougall and  
550 Harrison, 1999; Scibiorski et al., 2015), we consider the new zircon U-Pb ages  
551 ( $312\text{-}295$  Ma) of the pre- and syn-kinematic granite dykes as the maximum age, i.e.  
552 the initiation timing of the ductile dextral shearing along the XSZ, and previously  
553 published mica  $^{40}\text{Ar}/^{39}\text{Ar}$  ages ( $290\text{-}242$  Ma) for the MTSZ and NTF as the cooling  
554 ages of the ductile dextral shearing. It is worth noting that dextral shearing all along

555 the NTF-XSZ-MTSZ could have been active diachronously along different segments.  
556 The timing of earlier sinistral deformation along the XSZ cannot at this point be  
557 reliably constrained with the available data.

558 The WSZ represents a localized high strain belt inside the Central Tianshan (Fig.  
559 2). Within the WSZ, our new biotite  $^{40}\text{Ar}/^{39}\text{Ar}$  ages of 301-304 Ma were obtained  
560 from meta-sedimentary rocks showing sinistral kinematic fabrics (Fig. 10A-C). As the  
561 estimated deformation temperatures ( $>450\text{ }^{\circ}\text{C}$ ) of the WSZ are higher than the closure  
562 temperature of biotite argon system ( $335 \pm 50\text{ }^{\circ}\text{C}$ ), we therefore regard the newly  
563 acquired  $^{40}\text{Ar}/^{39}\text{Ar}$  ages as the cooling ages of the sinistral ductile deformation along  
564 the WSZ. Moreover, metamorphic zircons from a mylonitic greywacke of the Silurian  
565 Ahebulake Group within the WSZ yielded a mean age of  $\sim 312\text{ Ma}$  (He et al., 2018a).  
566 Thus, we infer that the sinistral shear of the WSZ likely took place during 312-301  
567 Ma. As to the dextral deformation, its timing and regional context are however  
568 difficult to be constrained.

569 Along the Baluntai Fault (BF), southern boundary of the Central Tianshan,  
570 granitic mylonites from the Baluntai, Kumishi and eastward vicinities were dated at  
571 311-248 Ma by  $^{40}\text{Ar}/^{39}\text{Ar}$  dating on mica, feldspar and hornblende (Yin and Nie, 1996;  
572 Laurent-Charvet et al., 2003; Yang et al., 2007; Y. Wang et al., 2008; Xu et al., 2011;  
573 Cai et al., 2012; Li et al., 2020). In the northern Kumishi area, a mylonitic gneissic  
574 granite was dated at  $304 \pm 2\text{ Ma}$  (Li et al., 2020), and a syn-kinematic potassic granite  
575 showing high-temperature superplastic creep deformation features yielded zircon  
576 U-Pb age of  $252 \pm 4\text{ Ma}$  (Wang et al., 2009). Dextral shear criteria are ubiquitous in

577 the mylonitic rocks along the Baluntai-Wuwamen-Kumishi section (Yin and Nie,  
578 1996; Laurent-Charvet et al., 2003; Wang et al., 2009, 2018; Tang et al., 2011; Xu et  
579 al., 2011; Cai et al., 2012; M. Wang et al., 2014; Zhong et al., 2015; Li et al., 2020).  
580 Thus, the dextral ductile shearing along the BF occurred during the latest  
581 Carboniferous to the end of Permian, and are hence comparable to the age span of the  
582 dextral shearing along the MTSZ-NTF. In addition, within and outside of the BF and  
583 in the MTSZ, sinistral shearing and N-S contractional deformation were previously  
584 suggested to occur at ~399-393 Ma and ~358-356 Ma, respectively (Allen et al., 1993;  
585 Deng et al., 2006; Yang et al., 2007; Li et al., 2020), prior to the dextral ductile  
586 shearing. Thus, the locally preserved sinistral kinematics recognized in the XSZ could  
587 be probably related also to this Devonian to early Carboniferous stage.

588 Farther westwards, the Nalati Fault (NF) also underwent dextral ductile  
589 deformation, which was dated by (1) mica  $^{40}\text{Ar}/^{39}\text{Ar}$  plateau ages of ~285-252 Ma in  
590 mylonites (Zhou et al., 2001; Wang et al., 2007c; de Jong et al., 2009), (2)  $277 \pm 3$  Ma  
591 zircon U-Pb age for a syn-kinematic intrusion in the Kekesu area (Wang et al., 2009),  
592 and (3) ~307 Ma to ~255 Ma metamorphic zircon U-Pb ages for strongly foliated  
593 early Paleozoic sandstones in the southern Nalati Range (Zhong et al., 2019).  
594 Therefore, the dextral ductile shearing along the NF took place from the late  
595 Carboniferous to end Permian, synchronous with the BF.

596

597 **6.3. Implications for late Paleozoic eastward tectonic wedging in SW CAO**

598 Strike-slip faults developed in the entire CAOBS and played an important role in  
599 building this large accretionary and collisional orogenic system (e.g., Sengör et al.,  
600 1993; Allen et al., 1993, 1995; Choulet et al., 2011; Li et al., 2017, 2018). There are  
601 different hypotheses concerning the formation mechanism and tectonic significance of  
602 these orogen-scale strike-slip shear zones. Many strike-slip faults subparallel to the  
603 orogens were considered to have formed during oblique subduction, duplicating and  
604 juxtaposing different fragments of the same arc, and shifting the magmatic front and  
605 overall geometry of orogens to form the oroclinal architecture of the Kazakhstan, SW  
606 CAOBS (Şengör et al., 1993; Şengör and Natal'in, 1996, 2014). Alternatively, a  
607 growing number of recent studies showed that the magmatic arcs in the SW CAOBS  
608 were formed by multi-stage subduction of various oceanic basins within the  
609 Paleo-Asian Ocean domain (e.g., Windley et al., 2007; Xiao et al., 2003, 2004;  
610 Wilhem et al., 2012), and that the orogen-parallel strike-slip faults more likely  
611 resulted from intra-continental tectonism after the Carboniferous oblique collision  
612 between the Siberian and Tarim cratons (Allen et al., 1993, 1995; Yin and Nie, 1996;  
613 Shu et al., 1999; Buslov et al., 2004; Wang et al., 2009; Pirajno, 2010).

614 In this context, Laurent-Charvet et al. (2002, 2003) and Cai et al. (2012)  
615 emphasized the anticlockwise rotation of the Junggar block during the early Permian,  
616 which resulted in dextral shearing along the NTF - MTSZ and sinistral transpression  
617 of the Irtysh Shear Zone (ISZ) (e.g., Glorie et al., 2012). Li et al. (2015) suggested  
618 that such coeval dextral and sinistral shearing was controlled by the lateral migration  
619 of various units within the CAOBS. Y. Wang et al. (2008) proposed that series of

620 dextral strike-slip shearing were results of post-orogenic eastward extrusion of the  
621 CAOB between the Siberian and Tarim Cratons. Similar eastward extrusion tectonics  
622 was also documented by paleomagnetic studies (e.g., Wang et al., 2007a; Choulet et  
623 al., 2011; Zhu et al., 2018, 2019b) suggesting that relative motions among the  
624 Kazakhstan-Yili, Junggar, Tu-Ha, Tarim and Siberia blocks during the late  
625 Carboniferous to Permian were characterized by significant anticlockwise rotations  
626 and accommodated by lateral displacement along major strike-slip faults (Wang et al.,  
627 2007a). The coeval horizontal displacements up to hundreds of kilometers along the  
628 large-scale shear zones (sinistral Irtysh and dextral NF-BF) favor an eastward tectonic  
629 wedging of Junggar-Yili-Central Tianshan in between the Siberia and Tarim blocks  
630 (Wang et al., 2007a).

631         Reliable geological and paleomagnetic data indicate that the Tianshan Orogen  
632 was formed by consumption of the Junggar-North Tianshan Ocean at ~310 Ma (e.g.,  
633 Han et al., 2010) and by welding of the Kazakhstan-Yili terrane with Tarim at  
634 ~320-310 Ma owing to the closure of the South Tianshan Ocean (e.g., Charvet et al.,  
635 2011; X.S. Wang et al., 2018) and associated back-arc oceanic basins (Wang et al.,  
636 2011, 2018). As mentioned above, although sinistral strike-slip kinematics recognized  
637 along the BF and MTSZ possibly resulted from the Devonian to early Carboniferous  
638 oblique subduction (Li et al., 2020), the more explicit and pervasive ductile strike-slip  
639 shearing around and within the Central Tianshan initiated almost simultaneously at  
640 312-310 Ma, and lasted until the end of Permian, except along the WSZ. Despite  
641 uncertainties on the timing and genesis of the locally preserved (and possible earlier)

642 dextral kinematics in the WSZ, we suggest that the latest Carboniferous to Permian  
643 (312-242 Ma) dextral strike-slip shearing along the MTSZ and BF, and the latest  
644 Carboniferous (312-301 Ma) sinistral strike-slip shearing along the WSZ occurred in  
645 post-orogenic intra-continental setting.

646 Combined with previous structural and paleomagnetic studies, our new results  
647 further confirm that the previously welded Yili - Central Tianshan - Junggar blocks  
648 simultaneously moved eastwards and wedged in between the Siberian and Tarim  
649 cratons (Fig. 15A). This eastward wedging was accommodated by synchronous  
650 dextral strike-slip shearing along the NF and BF, and then by the sinistral strike-slip  
651 shearing along the ISZ since ~284 Ma (Li et al., 2015). The dextral ductile strike-slip  
652 shearing along the NTF - MTSZ could be the result of differential eastward  
653 displacement rates of Junggar relative to the Yili - Central Tianshan blocks. Similarly,  
654 the sinistral WSZ probably resulted from relatively lower displacement velocity of the  
655 northern part of the Central Tianshan (north of the WSZ) with respect to its southern  
656 part (south of the WSZ), likely due to the backstop effect of the Tu-Ha terrane (Fig.  
657 15B). Meanwhile, it is noteworthy that the movement along the ISZ during earliest  
658 Permian was not well constrained due to lack of reliable geochronological data (e.g.,  
659 Hu et al., 2020). This interpretation could be tested with further kinematic and  
660 paleomagnetic studies to quantitatively assess the relative movement (rotation) rates  
661 between different tectonic units. Finally, the eastward tectonic wedging of the  
662 Kazakhstan-Yili, Central Tianshan and Junggar blocks was most likely triggered by  
663 the sub-E-W convergent orogenesis of the late Paleozoic Uralides related to the

664 collision between the Baltica and Siberia blocks (e.g., Biske and Seltmann, 2010;  
665 Ivanov et al., 2013).

666

## 667 **7. Conclusions**

668 (1) The Xiaergou shear zone along the northern boundary of the Central  
669 Tianshan is the connecting segment between the North Tianshan Fault and Main  
670 Tianshan Shear Zone. Large-scale and sample-scale structural and kinematic analyses  
671 indicate principally ductile dextral strike-slip shearing with locally preserved sinistral  
672 kinematics. The timing of dextral ductile shearing is dated at ~312-295 Ma by U-Pb  
673 dating of zircons from pre- and syn-kinematic granitic dykes.

674 (2) The Wulasitai shear zone is generally a WNW-ESE-trending high-strain belt  
675 developing in the interior of the Central Tianshan. Geometric, structural and  
676 kinematic analyses suggest predominantly sinistral strike-slip shearing associated with  
677 top-to-the-SW thrusting at the NW-SE bending segment of the shear zone, and dextral  
678 kinematics is locally preserved. Biotite  $^{40}\text{Ar}/^{39}\text{Ar}$  and metamorphic zircon U-Pb ages  
679 of meta-sedimentary rocks constrain the timing of the sinistral motion at ~312-301  
680 Ma.

681 (3) New structural and geochronological data from the Xiaergou and Wulasitai  
682 shear zones together with the regional geological and paleomagnetic data suggest that  
683 the latest Carboniferous to Permian ductile strike-slip shear zones in the Tianshan  
684 Orogen, SW CAOB, formed in a post-orogenic intra-continental setting, and likely

685 resulted from the eastward tectonic wedging of the Kazakhstan-Yili, Central Tianshan,  
686 Junggar blocks in between the Siberia and Tarim cratons.

687

## 688 **Acknowledgements**

689 We appreciate Mr. B. Wu (NJU) for his kind help in zircon LA-ICP-MS dating.  
690 We thank two anonymous reviewers for detailed and constructive comments and  
691 Editor-in-Chief Prof. C. Passchier for his editorial handling. This study was  
692 co-sponsored by the National Natural Science Foundation of China (42011530146,  
693 41772225, 41390445, 41222019), the Fundamental Research Funds for the Central  
694 Universities, the Open Fund of State Key Laboratory for Mineral Deposits Research  
695 (ZZKT-201603), the Fund for Scientific Research - Flanders (FWO, Bilateral Project  
696 VS06520N), LABEX VOLTAIRE (ANR - 10 - LABX - 100 - 01), Région Centre  
697 ARGON, and EQUIPEX PLANEX (ANR-11-EQPX-0036).

698

## 699 **Appendix: Analytical methods**

### 700 ***A.1. Zircon U-Pb dating***

701 Zircon grains from the samples 44-B and 49-C were concentrated via heavy  
702 liquids and magnetic separation techniques, and then hand-picked under a binocular  
703 microscope. Selected colorless zircons were mounted in epoxy resins and polished to  
704 approximately half-section thickness to expose the grains' center. In order to examine

705 the internal texture of the zircon grains, cathodoluminescence (CL) imaging was  
706 performed using the Mono CL 3+ Fluorescence Spectrometer (Gatan, USA) at  
707 Nanjing Hongchuang Analytical Institute.

708 Laser Ablation-Inductively Coupled Plasma-Mass Spectrometry (LA-ICP-MS)  
709 U-Pb dating of zircon was conducted at the State Key Laboratory for Mineral  
710 Deposits Research, Nanjing University, using an Agilent 7500s ICP-MS connected to  
711 a New Wave 213nm laser ablation system with an in-house sample cell. Zircon  
712 standard GEMOC GJ-1 ( $^{207}\text{Pb}/^{206}\text{Pb}$  age of  $608.5 \pm 1.5$  Ma; Jackson et al., 2004) was  
713 measured to correct fractionation, and the accuracy was monitored using zircon  
714 standard Mud Tank with an intercept age of  $732 \pm 5$  Ma (Black and Gulson, 1978).  
715 Samples were analyzed in runs of 15 analyses including 5 analyses on standard  
716 zircons and 10 analyses on samples of unknown ages. All analyses were carried out  
717 using a beam with a 32  $\mu\text{m}$  diameter and a repetition rate of 5 Hz.

718 U-Th-Pb isotopic ratios and ages were calculated from the raw signal data using  
719 the software package GLITTER. Correction for common Pb was performed via the  
720 EXCEL program ComPbCorr#3\_15G (Anderson, 2002). U-Pb Concordia diagrams  
721 and probability density curves of ages were conducted using ISOPLOT 3.0 (Ludwig,  
722 2003). Uncertainties are quoted at  $1\sigma$  for individual analyses and at  $2\sigma$  for mean ages.

723

#### 724 **A.2. Biotite $^{40}\text{Ar}/^{39}\text{Ar}$ dating**

725 Single grains of biotite were carefully handpicked under a binocular microscope

726 from 0.3-2.0 mm size fractions of crushed rock samples 01-B and 02-B. The biotite  
727 grains were then cleaned in distilled water and acetone before being weighed into Al  
728 foil envelopes for irradiation.

729 After neutron irradiation for 10 h in the CLICIT Cd-lined slot of the Corvallis  
730 Nuclear Reactor (Oregon State University, United States) along with the Fish Canyon  
731 Tuff sanidine standard ( $FCT\ 28.126 \pm 0.019\ Ma$  at  $2\sigma$ ) (Phillips et al., 2017),  
732  $^{40}Ar/^{39}Ar$  analyses were performed using a high-resolution Helix SFT mass  
733 spectrometer outfitted to a home-built  $CO_2$ -laser based extraction system featuring  
734 ultra-low argon blanks. Detailed operating conditions can be found in Corti et al.  
735 (2019).

736 Ages and isotopes ratios are plotted and tabulated at  $\pm 1\sigma$  and were calculated  
737 according to Scaillet (2000). Weighted mean ages (WMA) are calculated by  
738 inverse-variance weighting of the steps pooled in the weighted mean. Total-Gas ages  
739 (TGA) are calculated by summing all fractions released and by quadratically  
740 propagating the attached errors. Pooled age errors include procedural errors, and  
741 decay constants and isotope abundance errors.

742

#### 743 **Figure and Table captions:**

744 **Fig. 1.** (A) Simplified tectonic divisions of East Asia showing the location of the  
745 Central Asian Orogenic Belt (CAOB). EEC, East European Craton; KZN, Kazakhstan;  
746 QQ, Qaidam-Qinling (modified after Şengör et al., 1993; Jahn et al., 2000). (B)

747 Geological map of the SW CAOB, including major tectonic units and boundaries  
748 (after Windley et al., 2007; Choulet et al., 2011; Wang et al., 2012; Cao et al., 2017).  
749 Abbreviations correspond to: IKMT, Ishim-Kyrgyzstan Middle Tianshan; SKNT,  
750 Stepnyak-Kyrgyz North Tianshan; ACNT, Aktau-Chinese North Tianshan; NB, North  
751 Balkhash; BY, Balkhash-Yili; CY, Chu-Yili; BA, Baidalet-Akbastau; BC,  
752 Boshchekul-Chingiz; JB, Junggar-Balkhash; ZTS, Zharma-Tarbagatay-Saur; KM,  
753 Karamay; WJ, West Junggar; CNT, Chinese North Tianshan; CCT, Chinese Central  
754 Tianshan; BGD, Bogda; Bay, Bayinbulak; Gul, Guluogou; Kul, Kulehu; Wuw,  
755 Wuwamen. Numbers denote major faults: 1 = North Tianshan Fault (NTF), 2 = Main  
756 Tianshan Shear Zone (MTSZ), 3 = Nalati Fault (NF), 4 = Baluntai Fault (BF).

757

758 **Fig. 2.** Topographic and simplified geological map of the Central Tianshan and  
759 adjacent areas (modified from XIGMR, 2007), showing the locations of the Xiaergou  
760 shear zone (Fig. 3) and Wulasitai shear zone (Fig. 7). Abbreviations: NTF, North  
761 Tianshan Fault; MTSZ, Main Tianshan Shear Zone; NF, Nalati Fault; BF, Baluntai  
762 Fault; WSZ, Wulasitai Shear Zone.

763

764 **Fig. 3.** (A) Google Earth® Satellite image of the Xiaergou shear zone (XSZ). (B)  
765 Geological map of the XSZ (after 1:200,000 geological map of Houxia by XBGMR,  
766 1977a).

767

768 **Fig. 4.** (A) Structural map of the studied domain of the Xiaergou shear zone (XSZ)  
769 (see Fig. 3 for location) (after 1:200,000 geological map of Houxia by XBGMR,  
770 1977a), showing field structural data and sampling locations. (B) Stereonet plots  
771 (equal area lower hemisphere) of beddings (S0 poles), mylonitic foliations (S1 poles)  
772 and stretching lineation (L1) in the XSZ. (C) Cross-section across the XSZ showing  
773 the sample numbers and locations.

774

775 **Fig. 5.** Field photographs of representative structures in the Xiaergou shear zone. (A)  
776 Mylonitic foliation S1 and stretching lineation L1 in early Paleozoic granodiorite. (B)  
777 Mylonitic foliation S1 in the tuffaceous sandstone. (C) Mylonitic foliation S1 and  
778 stretching lineation L1 in Silurian marble. (D) Stretching lineation L1 in a leucocratic  
779 granite dyke. (E) strain localization and shear bands in early Paleozoic granodiorite  
780 indicating a dextral sense of shearing. (F) A sheath fold and A-type folds in a  
781 mylonitic marble demonstrating dextral strike-slip movement. (G) S-C fabrics in  
782 mylonitic marble suggesting a dextral sense of shear. (H) Sigmoid quartz clasts  
783 locally recognized in a greenschist showing sinistral sense of motion.

784

785 **Fig. 6.** Photomicrographs showing kinematic features of representative mylonites  
786 from the Xiaergou shear zone, thin sections were cut perpendicular to the foliation  
787 and parallel to the stretching lineation. (A) Bookshelf textures of plagioclase (Pl)  
788 porphyroclasts. (B-E) Asymmetric, sigmoid K-feldspar (Kfs) porphyroclasts and

789 pressure shadows indicating a dextral sense of shearing. (F) Locally recognized  
790 K-feldspar porphyroclast and pressure shadows suggesting sinistral motion.

791

792 **Fig. 7.** (A) Google Earth<sup>®</sup> Satellite image of the Wulasitai shear zone (WSZ). (B)  
793 Geological map of the WSZ (after 1:200,000 geological map of Baluntai by XBGMR,  
794 1977b).

795

796 **Fig. 8.** (A-C) Structural maps of the studied domains (see Fig. 7 for locations) along  
797 the Wulasitai shear zone (after 1:200,000 geological map of Baluntai by XBGMR,  
798 1977b and 1:50,000 geological map of Wulasitai by XBGMR, 2015) showing sample  
799 numbers and locations. (D) Stereonet plots (equal area lower hemisphere) of  
800 mylonitic foliation (S1 poles), stretching lineation (L1) and associated crenulation  
801 cleavages (L1').

802

803 **Fig. 9.** Field photographs of representative structures in the Wulasitai shear zone. (A)  
804 Mylonitic foliation S1 in meta-greywacke. (B-C) Stretching lineation L1 and  
805 crenulation cleavage L1' in paragneiss (B) and phyllite (C); Inset of Fig. 9B indicating  
806 the in situ partial melting and syn-kinematic transport of melts. (D-E) Mylonitic  
807 foliation S1 in meta-granite and syn-kinematic boudinage of felsic dyke (E). (F)  
808 Microfolds and shear bands indicating top-to-the-South shearing. (G) Asymmetric

809 microfolds in meta-rhyolite indicating sinistral shearing. (H) S-shaped intrafolial folds  
810 in meta-sandstone demonstrating a sinistral sense of shear, note the oblique relation  
811 between tails of S-type folds and main foliations. (I) Offset of syn-kinematic quartz  
812 veins in mylonitic granite suggesting a sinistral strike-slip movement.

813

814 **Fig. 10.** Photomicrographs of representative kinematic features of mylonites from the  
815 Wulasitai shear zone, thin sections were cut perpendicular to foliation and parallel to  
816 stretching lineation. (A) Biotite (Bt) mica fish indicating sinistral shearing. (B)  
817 Asymmetric K-feldspar (Kfs) porphyroclasts and pressure shadows and shear bands  
818 made of muscovite (Ms). (C-E)  $\sigma$ -type K-feldspar (Kfs) porphyroclasts and pressure  
819 shadows of biotite (Bt) and S-C fabrics (D), all indicating a sinistral sense of shear. (F)  
820 Sigmoid quartz (Qtz) and feldspar porphyroclasts and pressure shadows reflecting  
821 localized dextral motion, note the relation between pressure shadow and main  
822 foliations.

823

824 **Fig. 11.** Microstructural characteristics of dynamically recrystallized quartz grains in  
825 representative mylonites from the Xiaergou (A-C) and Wulasitai (D-F) shear zones.

826

827 **Fig. 12.** Plots of estimated temperatures v.s. latitudes of sampling sites for the  
828 ductilely deformed samples along the Xiaergou (A) and Wulasitai (B) shear zones.

829 Ranges of quartz recrystallization temperatures are based on Stipp et al. (2002a).

830 Abbreviations: BLG, bulging; SGR, sub-grain rotation; GBM, grain boundary  
831 migration.

832

833 **Fig. 13.** (A and E) Field occurrences and (B and F) photomicrographs of the sampled  
834 pre- and syn-tectonic granitic dykes in the Xiaergou shear zone. (C and G) CL images  
835 of the analyzed zircons from the granitic samples. (D and H) Concordia diagrams of  
836 U-Pb analytical results and mean age plots (insets).

837

838 **Fig. 14.** Photomicrographs (A-B),  $^{40}\text{Ar}/^{39}\text{Ar}$  age spectra (C-D) and chemical ratios  
839 (E-F) for the dated biotites of the meta-sedimentary rocks from the Wulasitai shear  
840 zone. Abbreviations: Bt = Biotite; Pl = Plagioclase; Qtz = Quartz.

841

842 **Fig. 15.** Interpretative sketch showing the intracontinental development of  
843 regional-scale strike-slip shear zones induced by relative motions and tectonic  
844 wedging of the Kazakhstan-Yili (K-Y), Central Tianshan (CT), Junggar (J) and Tu-Ha  
845 (T-H) blocks eastwards in between the Siberia and Tarim cratons during the latest  
846 Carboniferous. The shadowed areas around each block in (A) represent the loss of  
847 continental margins during convergence.

848

849 **Supplementary Table S1.** Textural descriptions of quartz dynamic recrystallization  
850 and temperature estimations for the mylonitic rocks from the Xiaergou and Wulasitai  
851 shear zones.

852

853 **Supplementary Table S2.** LA-ICP-MS zircon U-Pb analytical data for the  
854 syn-kinematic granitic rocks in the Xiaergou shear zone.

855

856 **Supplementary Table S3.** Laser total fusion  $^{40}\text{Ar}/^{39}\text{Ar}$  analytical data of single biotite  
857 grains from the meta-sedimentary rocks in the Wulasitai shear zone.

858

## 859 **References**

860 Alexeiev, D.V., Biske, Y.S., Wang, B., Djenchuraeva, A.V., Getman, O.F., Aristov,  
861 V.A., Kroner, A., Liu, H.S., Zhong, L.L., 2015. Tectono-stratigraphic framework  
862 and Palaeozoic evolution of the Chinese South Tianshan. *Geotectonics* 49,  
863 93-122.

864 Allen, C.R., 1965. Transcurrent faults in continental areas. *Philosophical Transactions*  
865 of the Royal Society A 258, 82-89.

866 Allen, M.B., Şengör, A.M.C., Natal'in, B.A., 1995. Junggar, Turfan and Alakol basins  
867 as Late Permian to Early Triassic extensional structures in a sinistral shear zone  
868 in the Altaid orogenic collage, Central-Asia. *Journal of the Geological Society*  
869 152, 327-338.

870 Allen, M.B., Windley, B.F., Zhang, C., 1993. Paleozoic collisional tectonics and

- 871 magmatism of the Chinese Tien Shan, Central Asia. *Tectonophysics* 220, 89-115.
- 872 Andersen, T., 2002. Correction of common Pb in U-Pb analyses that do not report  
873 <sup>204</sup>Pb. *Chemical Geology* 192, 59-79.
- 874 Avouac, J.P., Tapponnier, P., Bai, P., You, H., Wang, G., 1993. Active thrusting and  
875 folding along the northern Tien Shan, and Late Cenozoic rotation of the Tarim  
876 relative to the Junggar and Kazakhstan. *Journal of Geophysical Research* 98,  
877 6755-6804.
- 878 Beck, M.E., 1983. On the mechanism of tectonic transport in zones of oblique  
879 subduction. *Tectonophysics* 93, 1-11.
- 880 Bercovici, D., Ricard, Y., 2012. Mechanisms for the generation of plate tectonics by  
881 two-phase grain-damage and pinning. *Physics of the Earth and Planetary*  
882 *Interiors* 202-203, 27-55.
- 883 Berthé, D., Choukroune, P., Jegouzo, P., 1979. Orthogneiss, mylonite and non-coaxial  
884 deformation of granites: the example of the Shear zones and mylonites South  
885 Armorican Shear Zone. *Journal of Structural Geology* 1, 31-42.
- 886 Biske, Y.S., Seltmann, R., 2010. Paleozoic Tian-Shan as a transitional region between  
887 the Rheic and Urals-Turkestan oceans. *Gondwana Research* 17(2-3), 602-613.
- 888 Black, L.P., Gulson, B.L., 1978. The age of the Mud Tank carbonatite, Strangways  
889 Range, Northern Territory. Bureau of Mineral Resources. *Journal of Australian*  
890 *Geology and Geophysics* 3, 227-232.
- 891 Branquet, Y., Gumiaux, C., Sizaret, S., Barbanson, L., Wang, B., Cluzel, D., Li, G.R.,  
892 Delaunay, A., 2012. Synkinematic mafic/ultramafic sheeted intrusions:  
893 emplacement mechanism and strain restoration of the Permian Huangshan Ni-Cu  
894 ore belt (Eastern Tianshan, NW China). *Journal of Asian Earth Sciences* 56,  
895 240-257.
- 896 Buslov, M.M., Fujiwara, Y., Iwata, K., Semakov, N.N., 2004. Late Paleozoic-Early

- 897 Mesozoic geodynamics of Central Asia. *Gondwana Research* 7, 791-808.
- 898 Cai, Z.H., Xu, Z.Q., He, B.Z., Wang, R.R., 2012. Age and tectonic evolution of  
899 ductile shear zones in the eastern Tianshan-Beishan orogenic belt. *Acta*  
900 *Petrologica Sinica* 28, 1875-1895 (in Chinese with English abstract).
- 901 Cao, S.Y., Liu, J.L., Leiss, B., Neubauer, F., Genser, J., Zhao, C.Q., 2011.  
902 Oligo-Miocene shearing along the Ailao Shan-Red River shear zone: constraints  
903 from structural analysis and zircon U-Pb geochronology of magmatic rocks in  
904 the Diancang Shan massif, SE Tibet, China. *Gondwana Research* 19, 975-993.
- 905 Cao, S.Y., Neubauer, F., 2016. Deep crustal expressions of exhumed strike-slip fault  
906 systems: shear zone initiation on rheological boundaries. *Earth-Science Reviews*  
907 162, 155-176.
- 908 Cao, Y.C., Wang, B., Jahn, B.M., Cluzel, D., Shu, L.S., Zhong, L.L., 2017. Late  
909 Paleozoic arc magmatism in the southern Yili Block (NW China): insights to the  
910 geodynamic evolution of the Balkhash-Yili continental margin, Central Asian  
911 Orogenic Belt. *Lithos* 278, 111-125.
- 912 Charvet, J., Shu, L.S., Laurent-Charvet, S., 2007. Palaeozoic structural and  
913 geodynamic evolution of eastern Tianshan (NW China): welding of the Tarim  
914 and Junggar plates. *Episodes* 30, 162-186.
- 915 Charvet, J., Shu, L.S., Laurent-Charvet, S., Wang, B., Faure, M., Cluzel, D., Chen, Y.,  
916 de Jong, K., 2011. Palaeozoic tectonic evolution of the Tianshan belt, NW China.  
917 *Science China Earth Sciences* 54, 166-184.
- 918 Chen, W., Sun, S., Zhang, Y., Xiao, W.J., Wang, Y.T., Wang, Q.L., Jiang, L.Z., Yang,  
919 J.T., 2005.  $^{40}\text{Ar}/^{39}\text{Ar}$  geochronology of the Qiugemingtashi-Huangshan ductile  
920 shear zone in east Tianshan, Xinjiang, NW China. *Acta Geologica Sinica* 79,  
921 790-804 (in Chinese with English abstract).
- 922 Cherniak, D., Watson, E., 2003. Diffusion in Zircon. In: Hanchar J., Hoskin, P. (Eds).

- 923 Zircon. *Reviews in Mineralogy and Geochemistry* 53, 113-139.
- 924 Choulet, F., Chen, Y., Wang, B., Faure, M., Cluzel, D., Charvet, J., Lin, W., Xu, B.,  
925 2011. Late Paleozoic paleogeographic reconstruction of Western Central Asia  
926 based upon paleomagnetic data and its geodynamic implications. *Journal of*  
927 *Asian Earth Sciences* 42, 867-884.
- 928 Corfu, F., Hanchar, J.M., Hoskin, P.W.O., Kinny, P., 2003. Atlas of zircon textures.  
929 *Reviews in Mineralogy and Geochemistry* 53, 469-500.
- 930 Corti, G., Cioni, R., Franceschini, Z., Sani, F., Scaillet, S., Molin, P., Isola, I.,  
931 Mazzarini, F., Brune, S., Keir, D., Erbello, A., Muluneh, A., Illsley-Kemp, F.,  
932 Glerum, A., 2019. Aborted propagation of the Ethiopian rift caused by linkage  
933 with the Kenyan rift. *Nature Communications* 10, 1309. doi:  
934 10.1038/s41467-019-09335-2.
- 935 Cunningham, W.D., Mann, P., 2007. Tectonics of strike-slip restraining and releasing  
936 bends. Geological Society, London, Special Publications 290, 1-12.
- 937 Daly, M., Chorowicz, J., Fairhead, J., 1989. Rift basin evolution in Africa: the  
938 influence of reactivated steep basement shear zones. In: Cooper, M.A., Williams,  
939 G.D. (Eds.), *Inversion Tectonics*. Geological Society, London, Special  
940 Publications 44, pp. 309-334.
- 941 Davis, G.A., Lister, G.S., Reynolds, S.J., 1986. Structural evolution of the Whipple  
942 and South Mountains shear zones, southwestern United States. *Geology* 14, 7-10.
- 943 Davis, G.H., Reynolds, S.J., Kluth, C., 2011. *Structural geology of rocks and regions*,  
944 third ed. John Wiley & Sons, Hoboken.
- 945 De Grave, J., Buslov, M.M., Van den haute, P., 2007. Distant effects of India-Eurasia  
946 convergence and Mesozoic intracontinental deformation in Central Asia:  
947 constraints from apatite fission-track thermochronology. *Journal of Asian Earth*  
948 *Sciences* 29, 188-204.

- 949 de Jong, K., Wang, B., Faure, M., Shu, L.S., Cluzel, D., Charvet, J., Ruffet, G., Chen,  
950 Y., 2009. New  $^{40}\text{Ar}/^{39}\text{Ar}$  age constraints on the Late Palaeozoic tectonic  
951 evolution of the western Tianshan (Xinjiang, northwestern China), with emphasis  
952 on Permian fluid ingress. *International Journal of Earth Sciences* 98, 1239-1258.
- 953 Deng, S.T., Guo, Z.J., Zhang, Z.C., Liao, G.H., 2006. Timing of the formation of the  
954 Sangshuyuanzi ductile shear zone in the central segment of the South Tianshan  
955 and its tectonic significance. *Geology in China* 33, 641-647 (in Chinese with  
956 English abstract).
- 957 Dewey, J.F., Holdsworth, R.E., Strachan, R.A., 1998. Transpression and transtension.  
958 In: Holdsworth, R.E., Strachan, R.A., Dewey, J.F. (Eds.), *Continental  
959 Transpressional and Transtensional Tectonics*. Geological Society, London,  
960 Special Publications 135, pp. 1-14.
- 961 Dong, Y.P., Zhang, G.W., Neubauer, F., Liu, X.M., Hauzenberger, C., Zhou, D.W., Li,  
962 W., 2011. Syn- and post-collisional granitoids in the Central Tianshan orogen:  
963 geochemistry, geochronology and implications for tectonic evolution. *Gondwana  
964 Research* 20, 568-581.
- 965 Fossen, H., 2010. *Structural Geology*. Cambridge University Press, Cambridge.
- 966 Fossen, H., Tikoff, T.B., Teyssier, C.T., 1994, Strain modeling of transpressional and  
967 transtensional deformation. *Norsk Geologisk Tidsskrift* 74, 134-145.
- 968 Freund, R., 1974. Kinematics of transform and transcurrent faults. *Tectonophysics* 21,  
969 93-134.
- 970 Gao, J., Li, M.S., Xiao, X.C., Tang, Y.Q., He, G.Q., 1998. Paleozoic tectonic  
971 evolution of the Tianshan Orogen, northern China. *Tectonophysics* 287, 213-231.
- 972 Gao, J., Long, L.L., Klemd, R., Qian, Q., Liu, D.Y., Xiong, X.M., Su, W., Liu, W.,  
973 Wang, Y.T., Yang, F.Q., 2009. Tectonic evolution of the South Tianshan orogen  
974 and adjacent regions, NW China: geochemical and age constraints of granitoid

- 975 rocks. *International Journal of Earth Sciences* 98, 1221-1238.
- 976 Gao, J., Wang, X.S., Klemm, R., Jiang, T., Qian, Q., Mu, L.X., Ma, Y.Z., 2015. Record  
977 of assembly and breakup of Rodinia in the Southwestern Altaids: evidence from  
978 Neoproterozoic magmatism in the Chinese Western Tianshan Orogen. *Journal of*  
979 *Asian Earth Sciences* 113, 173-193.
- 980 Glorie, S., De Grave, J., 2016. Exhuming the Meso-Cenozoic Kyrgyz Tianshan and  
981 Siberian Altai-Sayan: a review based on low-temperature thermochronology.  
982 *Geoscience Frontiers* 7, 155-170.
- 983 Glorie, S., De Grave, J., Delvaux, D., Buslov, M.M., Zhimulev, F.I., Vanhaecke, F.,  
984 Elburg, M.A., 2012. Tectonic history of the Irtysh shear zone (NE Kazakhstan):  
985 new constraints from zircon U/Pb dating, apatite fission track dating and  
986 palaeostress analysis. *Journal of Asian Earth Sciences* 45, 138-149.
- 987 Han, B.F., Guo, Z.J., Zhang, Z.C., Zhang, L., Chen, J.F., Song, B., 2010. Age,  
988 geochemistry, and tectonic implications of a late Paleozoic stitching pluton in the  
989 North Tian Shan suture zone, western China. *Geological Society of America*  
990 *Bulletin* 122, 627-640.
- 991 Han, B.F., He, G.Q., Wang, X.C., Guo, Z.J., 2011. Late Carboniferous collision  
992 between the Tarim and Kazakhstan-Yili terranes in the Western segment of the  
993 South Tianshan Orogen, Central Asia, and implication for the Northern Xinjiang,  
994 western China. *Earth-Science Reviews* 109 (3-4), 74-93.
- 995 Han, Y., Zhao, G., 2018. Final amalgamation of the Tianshan and Junggar orogenic  
996 collage in the southwestern Central Asian Orogenic Belt: constraints on the  
997 closure of the Paleo-Asian Ocean. *Earth-Science Reviews* 186, 129-152.
- 998 Han, Y.G., Zhao, G.C., Sun, M., Eizenhöfer, P.R., Hou, W.Z., Zhang, X.R., Liu, Q.,  
999 Wang, B., Liu, D.X., Xu, B., 2016. Late Paleozoic subduction and collision  
1000 processes during the amalgamation of the Central Asian Orogenic Belt along the  
1001 South Tianshan suture zone. *Lithos* 246-247, 1-12.

- 1002 Harrison, T.M., C  lerier, J., Aikman, A.B., Hermann, J., Heitzler, M.T., 2009.  
1003 Diffusion of <sup>40</sup>Ar in muscovite. *Geochimica Cosmochimica Acta* 73, 1039-1051.
- 1004 Harrison, T. M., Duncan, I., McDougall, I., 1985. Diffusion of <sup>40</sup>Ar in biotite:  
1005 temperature, pressure and compositional effects. *Geochimica Cosmochimica*  
1006 *Acta* 49, 2461-2468.
- 1007 He, Z.Y., Klemd, R., Yan, L.L., Lu, T.Y., Zhang, Z.M., 2018b. Mesoproterozoic  
1008 juvenile crust in microcontinents of the Central Asian Orogenic Belt: evidence  
1009 from oxygen and hafnium isotopes in zircon. *Scientific Report* 8, 1-7.
- 1010 He, Z.Y., Klemd, R., Zhang, Z.M., Zong, K.Q., Sun, L.X., Tian, Z.L., Huang, B.T.,  
1011 2015. Mesoproterozoic continental arc magmatism and crustal growth in the  
1012 eastern Central Tianshan Arc Terrane of the southern Central Asian Orogenic  
1013 Belt: geochronological and geochemical evidence. *Lithos* 236-237, 74-89.
- 1014 He, Z.Y., Wang, B., Zhong, L.L., Zhu, X.Y., 2018a. Crustal evolution of the Central  
1015 Tianshan Block: Insights from zircon U-Pb isotopic and structural data from  
1016 meta-sedimentary and meta-igneous rocks along the Wulasitai - Wulanmoren  
1017 shear zone. *Precambrian Research* 314, 111-128.
- 1018 He, Z.Y., Zhang, Z.M., Zong, K.Q., Xiang, H., Chen, X.J., Xia, M.J., 2014. Zircon  
1019 U-Pb and Hf isotopic studies of the Xingxingxia Complex from Eastern Tianshan  
1020 (NW China): significance to the reconstruction and tectonics of the southern  
1021 Central Asian Orogenic Belt. *Lithos* 190-191, 485-499.
- 1022 Hirth, G., Teysier, C., Dunlap, W.J., 2001. An evaluation of quartzite flow laws based  
1023 on comparisons between experimentally and naturally deformed rocks.  
1024 *International Journal of Earth Sciences* 90, 77-87.
- 1025 Hu, A.Q., Jahn, B., Zhang, G.X., Chen, Y.B., Zhang, Q.F., 2000. Crustal evolution and  
1026 Phanerozoic crustal growth in northern Xinjiang: Nd isotopic evidence. Part I.  
1027 Isotopic characterization of basement rocks. *Tectonophysics* 328, 15-51.

- 1028 Hu, W., Li, P., Rosenbaum, G., Liu, J., Jourdan, F., Jiang, Y., Wu, Dan., Zhang, J.,  
1029 Yuan, C., Sun, M., 2020. Structural evolution of the eastern segment of the Irtysh  
1030 Shear Zone: implications for the collision between the East Junggar Terrane and  
1031 the Chinese Altai Orogen (northwestern China), *Journal of Structural Geology*  
1032 139, 104126.
- 1033 Hutton, D.H.W., 1988. Granite emplacement mechanisms and tectonic controls:  
1034 Inferences from deformation studies. *Transactions of the Royal Society of*  
1035 *Edinburgh-Earth Sciences* 79, 45-255.
- 1036 Holdsworth, R.E., Butler, C.A., Roberts, A.M., 1997. The recognition of reactivation  
1037 during continental deformation. *Journal of the Geological Society* 154, 73-78.
- 1038 Hutton, D.H.W., 1988. Granite emplacement mechanisms and tectonic controls:  
1039 Inferences from deformation studies. *Transactions of the Royal Society of*  
1040 *Edinburgh: Earth Sciences* 79, 245-255.
- 1041 Ivanov, K.S., Puchkov, V.N., Fyodorov, Y.N., Erokhin, Y.V., Pogromskaya, O.E., 2013.  
1042 Tectonics of the Urals and adjacent part of the West-Siberian platform basement:  
1043 Main features of geology and development. *Journal of Asian Earth Sciences* 72,  
1044 12-24.
- 1045 Jackson, S.E., Pearson, N.J., Griffin, W.L., Belousova, E.A., 2004. The application of  
1046 laser ablation-inductively coupled plasma-mass spectrometry to in-situ U-Pb  
1047 zircon geochronology. *Chemical Geology* 211, 47-69.
- 1048 Jahn, B.M., Wu, F.Y., Chen, B., 2000. Granitoids of the Central Asian Orogenic Belt  
1049 and continental growth in the Phanerozoic. *Transactions of the Royal Society of*  
1050 *Edinburgh: Earth Sciences* 91, 181-194.
- 1051 Jiang, T., Gao, J., Klemd, R., Qian, Q., Zhang, X., Xiong, X.M., Wang, X.S., Tan, Z.,  
1052 Chen, B.X., 2014. Paleozoic ophiolitic mélanges from the South Tianshan  
1053 Orogen, NW China: geological, geochemical and geochronological implications  
1054 for the geodynamic setting. *Tectonophysics* 612-613, 106-127.

- 1055 Laurent-Charvet, S., Charvet, J., Monié, P., Shu, L.S., 2003. Late Paleozoic strike-slip  
1056 shear zones in eastern central Asia (NW China): new structural and  
1057 geochronological data. *Tectonics* 22, 1009. doi:10.1029/2001TC901047.
- 1058 Laurent-Charvet, S., Charvet, J., Shu, L. S., Ma, R. S., Lu, H. F., 2002. Palaeozoic late  
1059 collisional strike-slip deformations in Tianshan and Altay, eastern Xinjiang, NW  
1060 China. *Terra Nova* 14, 249-256.
- 1061 Law, R.D., 2014. Deformation thermometry based on quartz *c*-axis fabrics and  
1062 recrystallization microstructures: a review. *Journal of Structural Geology* 66,  
1063 129-161.
- 1064 Lei, R.X., Wu, C.Z., Gu, L.X., Zhang, Z.Z., Chi, G.X., Jiang, Y.H., 2011. Zircon U-Pb  
1065 chronology and Hf isotope of the Xingxingxia granodiorite from the Central  
1066 Tianshan zone (NW China): implications for the tectonic evolution of the  
1067 southern Altaids. *Gondwana Research* 20, 582-593.
- 1068 Leloup, P.H., Lacassin, R., Tapponnier, P., Scharer, U., Zhong, D.L., Liu, X.H., Zhang,  
1069 L.S., Ji, S.C., Phan, T., 1995. The Ailao Shan-Red River shear zone  
1070 (Yunnan,China), tertiary transform boundary of Indochina. *Tectonophysics* 251,  
1071 3-84.
- 1072 Li, X.D., Liu, J.B., 1997. Tectonic analysis of Laerdun Daban of West Tianshan  
1073 Mountains, China. *Xinjiang Geology* 15, 371-378 (in Chinese with English  
1074 abstract).
- 1075 Li, P.F., Sun, M., Rosenbaum, G., Cai, K.D., Yu, Y., 2015. Structural evolution of the  
1076 Irtyshe Shear Zone (northwestern China) and implications for the amalgamation  
1077 of arc systems in the Central Asian Orogenic Belt. *Journal of Structural Geology*  
1078 80, 142-156.
- 1079 Li, P.F., Sun, M., Rosenbaum, G., Cai, K.D., Yuan, C., Jourdan, F., Xia, X.P., Jiang,  
1080 Y.D., Zhang, Y.Y., 2020. Tectonic evolution of the Chinese Tianshan Orogen

- 1081 from subduction to arc-continent collision: Insight from polyphase deformation  
1082 along the Gangou section, Central Asia. Geological Society of America Bulletin,  
1083 doi: <https://doi.org/10.1130/B35353.1>.
- 1084 Li, P.F., Sun, M., Rosenbaum, G., Jourdan, F., Li, S., Cai, K.D., 2017. Late Paleozoic  
1085 closure of the Ob-Zaisan Ocean along the Irtysh shear zone (NW China):  
1086 Implications for arc amalgamation and oroclinal bending in the Central Asian  
1087 orogenic belt. Geological Society of America Bulletin 129(5-6), 547-569.
- 1088 Li, P.F., Sun, M., Rosenbaum, G., Yuan, C., Safonova, I., Cai, K.D., Jiang, Y.D.,  
1089 Zhang, Y.Y., 2018. Geometry, kinematics and tectonic models of the Kazakhstan  
1090 Orocline, Central Asian Orogenic Belt. Journal of Asian Earth Sciences 153,  
1091 42-56.
- 1092 Lin, W., Chu, Y., Ji, W.B., Zhang, Z.P., Shi, Y.H., Wang, Z.Y., Li, Z., Wang, Q.C.,  
1093 2013. Geochronological and geochemical constraints for a middle Paleozoic  
1094 continental arc on the northern margin of the Tarim block: implications for the  
1095 Paleozoic tectonic evolution of the South Chinese Tianshan. Lithosphere 5,  
1096 355-381.
- 1097 Liu, J.L., Chen, X.Y., Tang, Y., Song, Z.J., Wang, W., 2020. The Ailao Shan-Red  
1098 River shear zone revisited: timing and tectonic implications. Geological Society  
1099 of America Bulletin 132, 1165-1182.
- 1100 Liu, H.S., Wang, B., Shu, L.S., Jahn, B.M., Lizuka, Y., 2014. Detrital zircon ages of  
1101 Proterozoic meta-sedimentary rocks and Paleozoic sedimentary cover of northern  
1102 Yili Block: implications for the tectonics of microcontinents in the Central Asian  
1103 Orogenic Belt. Precambrian Research 252, 209-222.
- 1104 Liu, T.L., Zhang, B., Han, B.F., Wang, M., Cai, K.D., Qu, J.F., 2020. Structural,  
1105 Kinematic and Geochronological Study of the Main Tianshan Shear Zone in the  
1106 Borohoro Ranges, NW China. Acta Geologica Sinica, in press.
- 1107 Long, L.L., Gao, J., Klemd, R., Beier, C., Qian, Q., Zhang, X., Wang, J.B., Jiang, T.,

- 1108 2011. Geochemical and geochronological studies of granitoid rocks from the  
1109 Western Tianshan Orogen: implications for continental growth in the  
1110 southwestern Central Asian Orogenic Belt. *Lithos* 126, 321-340.
- 1111 Ludwig, K.R., 2003. *ISOPLLOT 3.00: a Geochronology Toolkit for Microsoft Excel*.  
1112 Berkeley Geochronological Center Special Publication, Berkeley.
- 1113 Ludwig, K.R., 2012. *User's Manual for Isoplot 3.75. A Geochronological Toolkit for*  
1114 *Microsoft Excel: Special Publication No. 5, Berkeley Geochronology Center,*  
1115 *Berkeley, California.*
- 1116 Ma, X.X., Shu, L.S., Meert, J.G., Li, J.Y., 2014. The Paleozoic evolution of Central  
1117 Tianshan: geochemical and geochronological evidence. *Gondwana Research* 25,  
1118 797-819.
- 1119 Mann, P., 2007. Global catalogue, classification and tectonic origin of active  
1120 restraining-and releasing bends, on strike-slip fault systems. In: Cunningham,  
1121 W.D., Mann, P. (Eds.), *Tectonics of Strike-Slip Restraining and Releasing Bends*.  
1122 Geological Society, London, Special Publications 290, pp. 13-142.
- 1123 McDougall, I., Harrison M., 1999. *Geochronology and thermochronology by the*  
1124  *$^{40}\text{Ar}/^{39}\text{Ar}$  method*, Oxford University Press, New York.
- 1125 Metelkin, D.V., Vernikovskiy, V.A., Kazansky, A. Yu., Wingate, M.T.D., 2010. Late  
1126 Mesozoic tectonics of Central Asia based on paleomagnetic evidence. *Gondwana*  
1127 *Research* 18, 400-419.
- 1128 Molnar, P., Tapponnier, P., 1975. Cenozoic tectonics of Asia: effects of a continental  
1129 collision. *Science* 189, 419-426.
- 1130 Moore, J.M., 1979. Tectonics of the Najd transcurrent fault system, Saudi Arabia.  
1131 *Journal of the Geological Society* 136, 441-452.
- 1132 Onstott, T.C., Hargraves, R.B., 1981. Proterozoic transcurrent tectonics:  
1133 palaeomagnetic evidence from Venezuela and Africa. *Nature* 289, 131-136.

- 1134 Passchier, C.W., Trouw, R.A.J., 2005. *Microtectonics*, second ed. Springer-Verlag,  
1135 Berlin.
- 1136 Passchier, C.W., Zhang, J.S., Konopásek, J., 2005. Geometric aspects of synkinematic  
1137 granite intrusion into a ductile shear zone - An example from the Yunmengshan  
1138 core complex, northern China. In: Bruhn, D., Burlini, L. (Eds.), *High-Strain  
1139 Zones: Structure and Physical Properties*. Geological Society, London, Special  
1140 Publications 245, pp. 65-80.
- 1141 Phillips, D., Matchan, L., 2013. Ultra-high precision  $^{40}\text{Ar}/^{39}\text{Ar}$  ages for Fish Canyon  
1142 Tuff and Alder Creek Rhyolite sanidine: new dating standards required?  
1143 *Geochimica et Cosmochimica Acta* 121, 229-239.
- 1144 Phillips, D., Matchan, E.L., Honda, M., Kuiper, K.F., 2017. Astronomical calibration  
1145 of  $^{40}\text{Ar}/^{39}\text{Ar}$  reference minerals using high-precision, multi-collector (ARGUSVI)  
1146 mass spectrometry. *Geochimica et Cosmochimica Acta* 196, 351-369.
- 1147 Pirajno, F., 2010. Intracontinental strike-slip faults, associated magmatism, mineral  
1148 systems and mantle dynamics: examples from NW China and Altay-Sayan  
1149 (Siberia). *Journal of Geodynamics* 50, 325-346.
- 1150 Pitcher, W.S., 1997. *The Nature and Origin of Granite* (2nd ed.). Chapman and Hall,  
1151 London. 387pp.
- 1152 Qian, Q., Gao, J., Klemd, R., He, G.Q., Song, B., Liu, D.Y., Xu, R.H., 2009. Early  
1153 Paleozoic tectonic evolution of the Chinese South Tianshan Orogen: constraints  
1154 from SHRIMP zircon U-Pb geochronology and geochemistry of basaltic and  
1155 dioritic rocks from Xiata, NW China. *International Journal of Earth Sciences* 98,  
1156 551-569.
- 1157 Ramsay, J. G., 1980. Shear zone geometry: a review. *Journal of Structural Geology* 2,  
1158 83-99.
- 1159 Sanderson, D.J., Marchini, W., 1984. Transpression. *Journal of Structural Geology* 6,

- 1160 449-458.
- 1161 Scaillet, S., 2000. Numerical error analysis in  $^{40}\text{Ar}/^{39}\text{Ar}$  dating. *Chemical Geology*  
1162 162, 269-298.
- 1163 Scibiorski, E., Tohver, E., Jourdan, F., 2015. Rapid cooling and exhumation in the  
1164 western part of the Mesoproterozoic Albany-Fraser Orogen, Western Australia.  
1165 *Precambrian Research* 265, 232-248.
- 1166 Searle, M.P., 2006. Role of the Red River shear zone, Yunnan and Vietnam, in the  
1167 continental extrusion of SE Asia: *Journal of the Geological Society* 163,  
1168 1025-1036.
- 1169 Şengör, A.M.C., Natal'in, B.A., 1996. Paleotectonics of Asia: fragments of a synthesis.  
1170 In: Yin, A., Harrison, M. (Eds.), *The Tectonic Evolution of Asia*. Cambridge  
1171 University Press, Cambridge, pp. 486-640.
- 1172 Şengör, A.M.C., Natal'in, B.A., Burtman, V.S., 1993. Evolution of the Altiid tectonic  
1173 collage and Palaeozoic crustal growth in Eurasia. *Nature* 364, 299-307.
- 1174 Şengör, A.M.C., Natal'in, B.A., van der Voo, R., Sunal, G., 2014. A new look at the  
1175 Altaiids: A superorogenic complex in northern and central Asia as a factory of  
1176 continental crust. Part II: palaeomagnetic data, reconstructions, crustal growth  
1177 and global sea-level. *Austrian Journal of Earth Sciences* 107(2), 131-181.
- 1178 Shi, Y.R., Liu, D.Y., Zhang, Q., Jian, P., Zhang, F.Q., Miao, L.C., 2007. SHRIMP  
1179 zircon U-Pb dating of the Gangou granitoids, Central Tianshan Mountains,  
1180 Northwest China and tectonic significances. *Chinese Science Bulletin* 52,  
1181 1507-1516.
- 1182 Shu, L.S., Charvet, J., Guo, L.Z., Lu, H.F., Laurent-Charvet, S., 1999. A large-scale  
1183 Palaeozoic dextral ductile strike-slip zone: the Aqqikkudug-Weiya zone along the  
1184 northern margin of the Central Tianshan belt, Xinjiang, NW China. *Acta*  
1185 *Geologica Sinica* 73, 148-162.

- 1186 Shu, L.S., Charvet, J., Lu, H.F., Laurent, S.C., 2002. Paleozoic accretion-collision  
1187 events and kinematics of ductile deformation in the eastern part of the  
1188 southern-central Tianshan belt, China. *Acta Geologica Sinica* 76, 308-323.
- 1189 Shu, L.S., Zhu, W.B., Wang, B., Wu, C.Z., Ma, D.S., Ma, X.X., Ding, H.F., 2013. The  
1190 formation and evolution of ancient blocks in Xinjiang. *Geology in China* 40,  
1191 43-60 (in Chinese with English abstract).
- 1192 Stipp, M., Stünitz, H., Heilbronner, R., Schmid, S.M., 2002a. The eastern Tonale fault  
1193 zone: a 'natural laboratory' for crystal plastic deformation of quartz over a  
1194 temperature range from 250 °C to 700 °C. *Journal of Structural Geology* 24,  
1195 1861-1884.
- 1196 Stipp, M., Stünitz, H., Heilbronner, R., Schmid, S.M., 2002b. Dynamic  
1197 recrystallization of quartz: correlation between natural and experimental  
1198 conditions. In: De Meer, S., Drury, M.R., De Bresser, J.H.P., Pennock, G.M.  
1199 (Eds.), *Deformation Mechanisms, Rheology and Tectonics: Current Status and  
1200 Future Perspectives*. Geological Society, London, Special Publications 200, pp.  
1201 171-190.
- 1202 Sylvester, A.G., 1988. Strike-slip faults. *Geological Society of America Bulletin* 100,  
1203 1666-1703.
- 1204 Tang, Z.M., Cai, Z.H., Wang, Z.X., Chen, F.Y., 2011. Deformational characteristics of  
1205 ductile shear zones in northern and southern margins of eastern central Tianshan.  
1206 *Geology in China* 38, 970-979 (in Chinese with English abstract).
- 1207 Tapponnier, P., Lacassin, R., Leloup, P.H., Scharer, U., Zhong, D.L., Wu, H.W., Liu,  
1208 X.H., Ji, S.C., Zhang, L.S., Zhong, J.Y., 1990. The Ailao Shan Red River  
1209 metamorphic belt tertiary left-lateral shear between Indochina and south China.  
1210 *Nature* 343, 431-437.
- 1211 Tikoff, B., Teyssier, C., 1994. Strain modeling of displacement-field partitioning in  
1212 transpressional orogens. *Journal of Structural Geology* 16, 1575-1588.

- 1213 Wali, G., Wang, B., Cluzel, D., Zhong, L.L., 2018. Carboniferous-Early Permian  
1214 magmatic evolution of the Bogda Range (Xinjiang, NW China): implications for  
1215 the Late Paleozoic accretionary tectonics of the SW Central Asian Orogenic Belt.  
1216 *Journal of Asian Earth Sciences* 153, 238-251.
- 1217 Wang, B., Chen, Y., Zhan, S., Shu, L.S., Faure, M., Cluzel, D., Charvet, J.,  
1218 Laurent-Charvet, S., 2007a. Primary Carboniferous and Permian paleomagnetic  
1219 results from the Yili Block (NW China) and their implications on the  
1220 geodynamic evolution of Chinese Tianshan Belt. *Earth and Planetary Science*  
1221 *Letters* 263, 288-308.
- 1222 Wang, B., Cluzel, D., Jahn, B.-M., Shu, L., Chen, Y., Zhai, Y., Branquet, Y.,  
1223 Barbanson, L., Sizaret, S., 2014b. Late Paleozoic pre- and syn-kinematic plutons  
1224 of the Kangguer-Huangshan Shear zone: inference on the tectonic evolution of  
1225 the eastern Chinese north Tianshan. *American Journal of Science* 314, 43-79.
- 1226 Wang, B., Cluzel, D., Shu, L.S., Faure, M., Charvet, J., Chen, Y., Meffre, S., de Jong,  
1227 K., 2009. Evolution of calc-alkaline to alkaline magmatism through  
1228 Carboniferous convergence to Permian transcurrent tectonics, western Chinese  
1229 Tianshan. *International Journal of Earth Sciences* 98, 1275-1298.
- 1230 Wang, B., Faure, M., Cluzel, D., Shu, L.S., Charvet, J., Meffre, S., 2006. Late  
1231 Paleozoic tectonic evolution of the northern West Tianshan, NW China.  
1232 *Geodinamica Acta* 19, 237-247.
- 1233 Wang, B., Faure, M., Shu, L.S., Cluzel, D., Charvet, J., de Jong, K., Chen, Y., 2008.  
1234 Paleozoic geodynamic evolution of the Yili Block, Western Chinese Tianshan.  
1235 *Bulletin de la Société Géologique de France* 179, 483-490.
- 1236 Wang, B., Faure, M., Shu, L., de Jong, K., Charvet, J., Cluzel, D., Jahn, B.M., Chen,  
1237 Y., Ruffet, G., 2010. Structural and geochronological study of high-pressure  
1238 metamorphic rocks in the Kekesu section (northwestern China): implications for  
1239 the late Paleozoic tectonics of the Southern Tianshan. *The Journal of Geology*

- 1240 118, 59-77.
- 1241 Wang, B., Liu, H., Shu, L., Jahn, B.M., Chung, S.L., Zhai, Y., Liu, D., 2014a. Early  
1242 Neoproterozoic crustal evolution in northern Yili Block: insights from migmatite,  
1243 orthogneiss and leucogranite of the Wenquan metamorphic complex in the NW  
1244 Chinese Tianshan. *Precambrian Research* 242, 58-81.
- 1245 Wang, B., Shu, L.S., Cluzel, D., Faure, M., Charvet, J., 2007b. Geochemical  
1246 constraints on Carboniferous volcanic rocks of Yili Block (Xinjiang, NW China);  
1247 implication on tectonic evolution of Western Tianshan. *Journal of Asian Earth  
1248 Sciences* 29, 148-159.
- 1249 Wang, B., Shu, L.S., Faure, M., Cluzel, D., Charvet, J., 2007c. Paleozoic tectonism  
1250 and magmatism of Kekesu-Qiongkushitai section in southwestern Chinese  
1251 Tianshan and their constraints on the age of the orogeny. *Acta Petrologica Sinica  
1252* 23, 1354-1368.
- 1253 Wang, B., Shu, L., Faure, M., Jahn, B.M., Cluzel, D., Charvet, J., Chung, S.L., Meffre,  
1254 S., 2011. Paleozoic tectonics of the southern Chinese Tianshan: Insights from  
1255 structural, chronological and geochemical studies of the Heiyingshan ophiolitic  
1256 mélange (NW China). *Tectonophysics* 497, 85-104.
- 1257 Wang, B., Zhai, Y.Z., Kapp, P., de Jong, K., Zhong, L.L., Liu, H.S., Ma, Y.Z., Gong,  
1258 H.J., Geng, H.Y., 2018. Accretionary tectonics of back-arc oceanic basins in the  
1259 South Tianshan: insights from structural, geochronological, and geochemical  
1260 studies of the Wuwamen ophiolite mélange. *Geological Society of America  
1261 Bulletin* 130, 284-306.
- 1262 Wang, M., Zhang, J.J., Qi, G.W., Zheng, Y., Liu, K., 2014. An Early Silurian ductile  
1263 deformation event in the Sangshuyuanzi shear zone, the southern margin of the  
1264 Central Tianshan belt, and its geological significance. *Acta Petrologica Sinica* 30,  
1265 3051-3061 (in Chinese with English abstract).

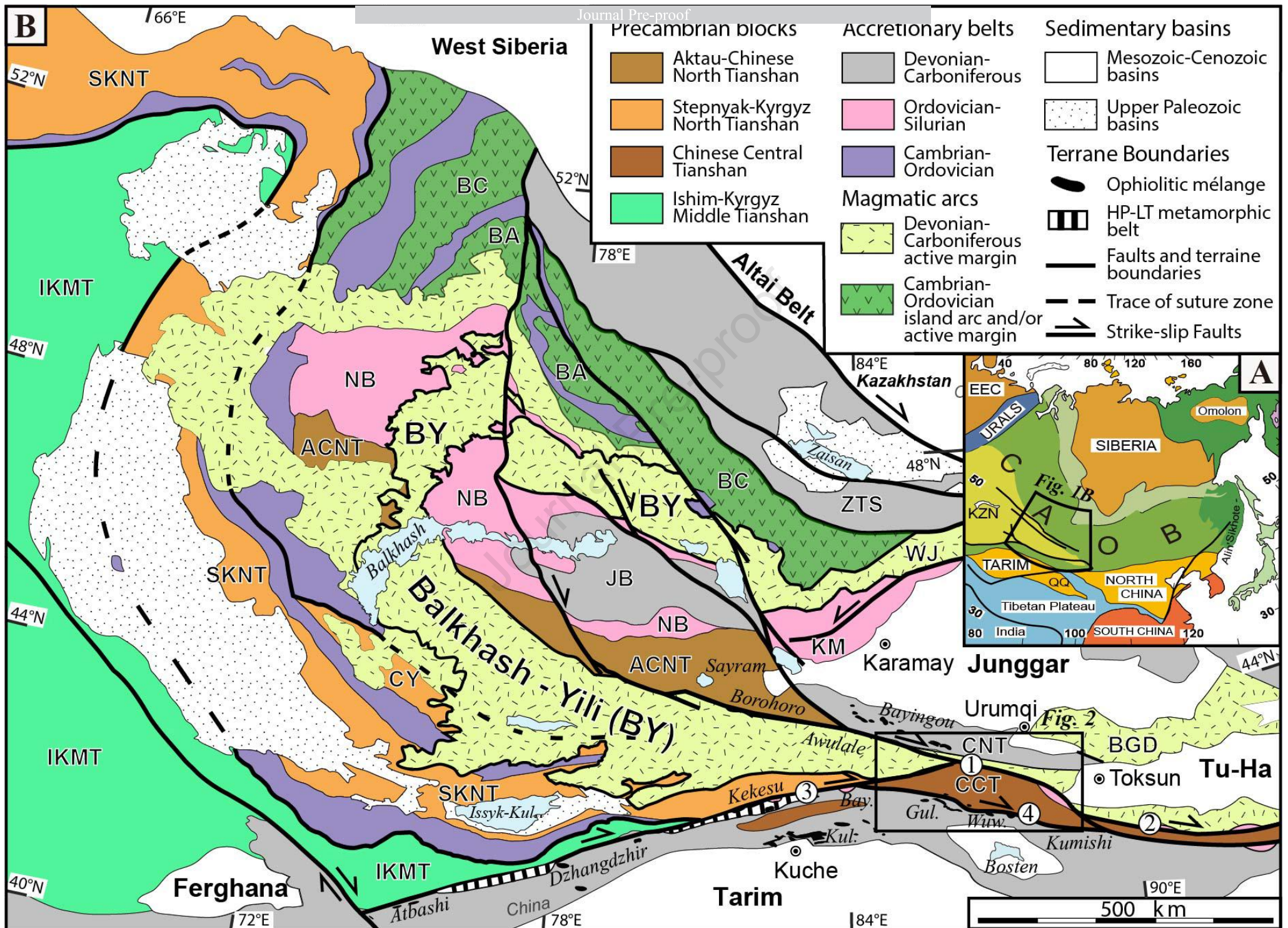
- 1266 Wang, X.S., Gao, J., Klemd, R., Jiang, T., Li, J.L., Zhang, X., Xue, S.C., 2017. The  
1267 Central Tianshan Block: A microcontinent with a Neoproterozoic-Paleoproterozoic  
1268 basement in the southwestern Central Asian Orogenic Belt. *Precambrian*  
1269 *Research* 295, 130-150.
- 1270 Wang, X.S., Klemd, R., Gao, J., Jiang, T., Li, J.L., Xue, S.C., 2018. Final assembly of  
1271 the Southwestern Central Asian Orogenic Belt as constrained by the evolution of  
1272 the South Tianshan Orogen: links with Gondwana and Pangea. *Journal of*  
1273 *Geophysical Research: Solid Earth* 123, 7361-7388.
- 1274 Wang, Y., Li, J.Y., Sun, G.H., 2008. Postcollisional eastward extrusion and tectonic  
1275 exhumation along the eastern Tianshan Orogen, Central Asia: constraints from  
1276 dextral strike-slip motion and  $^{40}\text{Ar}/^{39}\text{Ar}$  geochronological evidence. *The Journal*  
1277 *of Geology* 116, 599-618.
- 1278 Wilhem, C., Windley, B.F., Stampfli, G.M., 2012. The Altaids of Central Asia: a  
1279 tectonic and evolutionary innovative review. *Earth-Science Reviews* 113,  
1280 303-341.
- 1281 Wilson, J.T., 1965. A new class of faults and their bearing on continental drift. *Nature*  
1282 207, 343-347.
- 1283 Windley, B.F., Alexeiev, D., Xiao, W.J., Kröner, A., Badarch, G., 2007. Tectonic  
1284 models for accretion of the Central Asian Orogenic Belt. *Journal of the*  
1285 *Geological Society* 164, 31-47.
- 1286 XBGMR (Xinjiang Bureau of Geology and Mineral Resources), 1977a. 1:200,000  
1287 Geological map, Houxia sheet (K-45-X).
- 1288 XBGMR (Xinjiang Bureau of Geology and Mineral Resources), 1977b. 1:200,000  
1289 Geological map, Baluntai sheet (K-45-IX).
- 1290 XBGMR (Xinjiang Bureau of Geology and Mineral Resources), 2015. 1:50,000  
1291 Geological map, Wulasitai sheet (K45E007011).

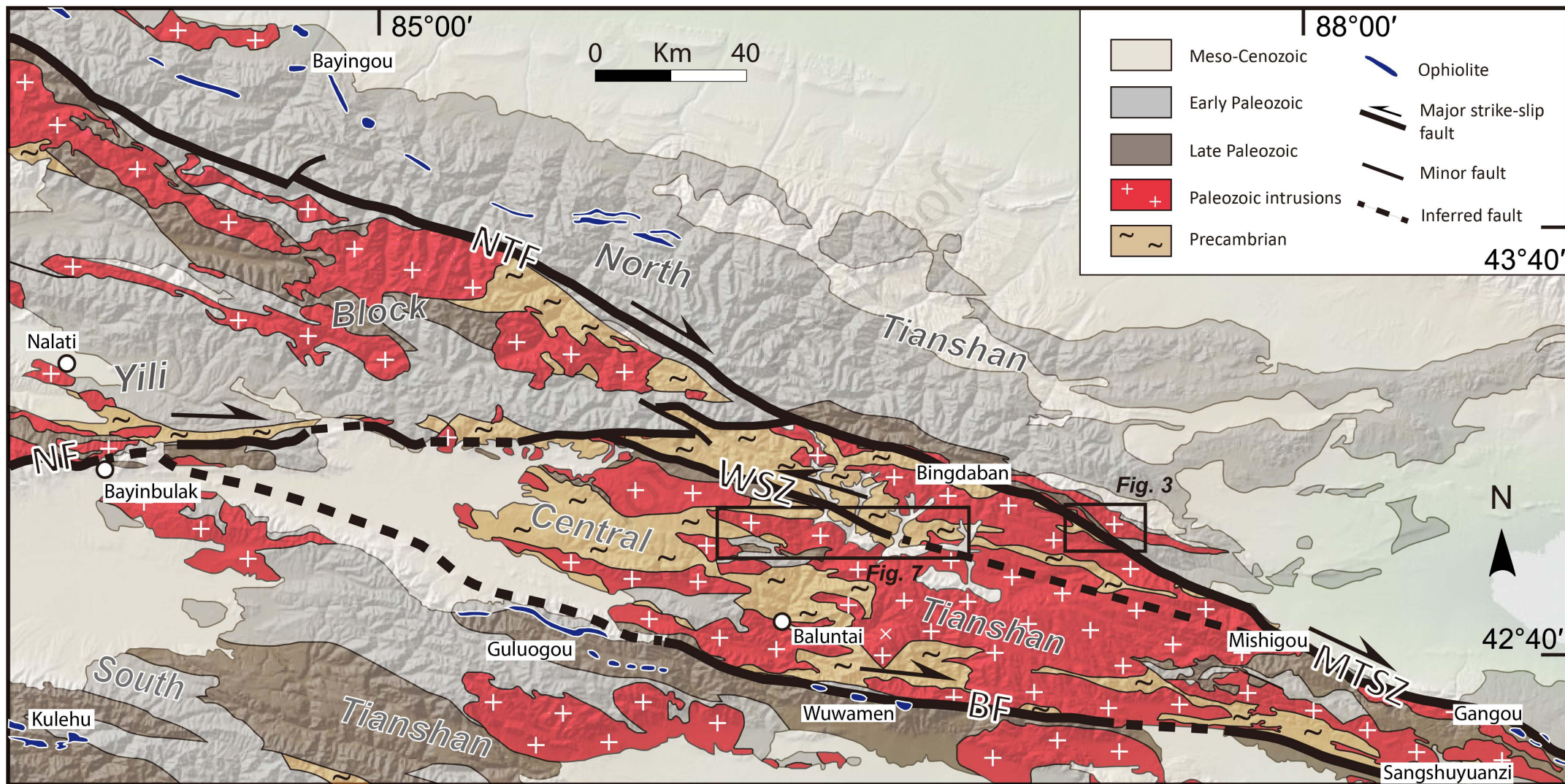
- 1292 XBGMR (Xinjiang Bureau of Geology and Mineral Resources), 1993. Regional  
1293 Geology of Xinjiang Uygur Autonomy Region. Geology Publishing House,  
1294 Beijing, 841 pp (in Chinese).
- 1295 XIGMR (Xi'an Institute of Geology and Mineral Resources), 2007. Chinese Tianshan  
1296 and its Adjacent Area 1:1 000,000. In: Centre, X.a.G.S. (Ed.)-Geological  
1297 Publishing House, Beijing.
- 1298 Xiao, W., Windley, B.F., Allen, M.B., Han, C., 2013. Paleozoic multiple accretionary  
1299 and collisional tectonics of the Chinese Tianshan orogenic collage. *Gondwana*  
1300 *Research* 23, 1316-1341.
- 1301 Xiao, W.J., Windley, B.F., Hao, J., Zhai, M.G., 2003. Accretion leading to collision  
1302 and the Permian Solonker suture, Inner Mongolia, China: termination of the  
1303 central Asian orogenic belt. *Tectonics* 22, 1069. doi:10.1029/2002TC1484.
- 1304 Xiao, W.J., Zhang, L.C., Qin, K.Z., Sun, S., Li, J.L., 2004. Paleozoic accretionary and  
1305 collisional tectonics of the Eastern Tianshan (China): implications for the  
1306 continental growth of central Asia. *American Journal of Science* 304, 370-395.
- 1307 Xiao, X.C., Tang, Y.Q., Feng, Y.M., Zhu, B.Q., Li, J.Y., Zhao, M., 1992. Tectonic  
1308 Evolution of the Northern Xinjiang and its adjacent regions. Geological  
1309 Publishing House, Beijing, 190 pp (in Chinese).
- 1310 Xu, X.W., Ma, T.L., Sun, L.Q., Cai, X.P., 2003. Characteristics and dynamic origin of  
1311 the large-scale Jiaoluoage ductile compressional zone in the eastern Tianshan  
1312 Mountains, China. *Journal of Structural Geology* 25, 1901-1915.
- 1313 Xu, X.Y., Wang, H.L., Li, P., Chen, J.L., Ma, Z.P., Zhu, T., Wang, N., Dong, Y.P.,  
1314 2013. Geochemistry and geochronology of Paleozoic intrusions in the Nalati  
1315 (Narati) area in western Tianshan, Xinjiang, China: Implications for Paleozoic  
1316 tectonic evolution. *Journal of Asian Earth Sciences* 72, 33-62.
- 1317 Xu, Z.Q., Li, S.T., Zhang, J.X., Sui, Y.J., He, B.Z., Li, H.B., Lin, C.S., Cai, Z.H., 2011.

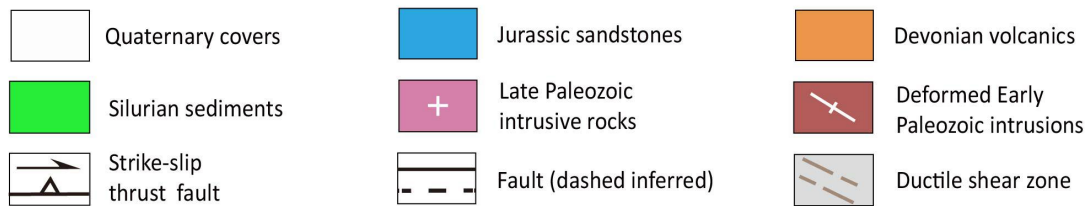
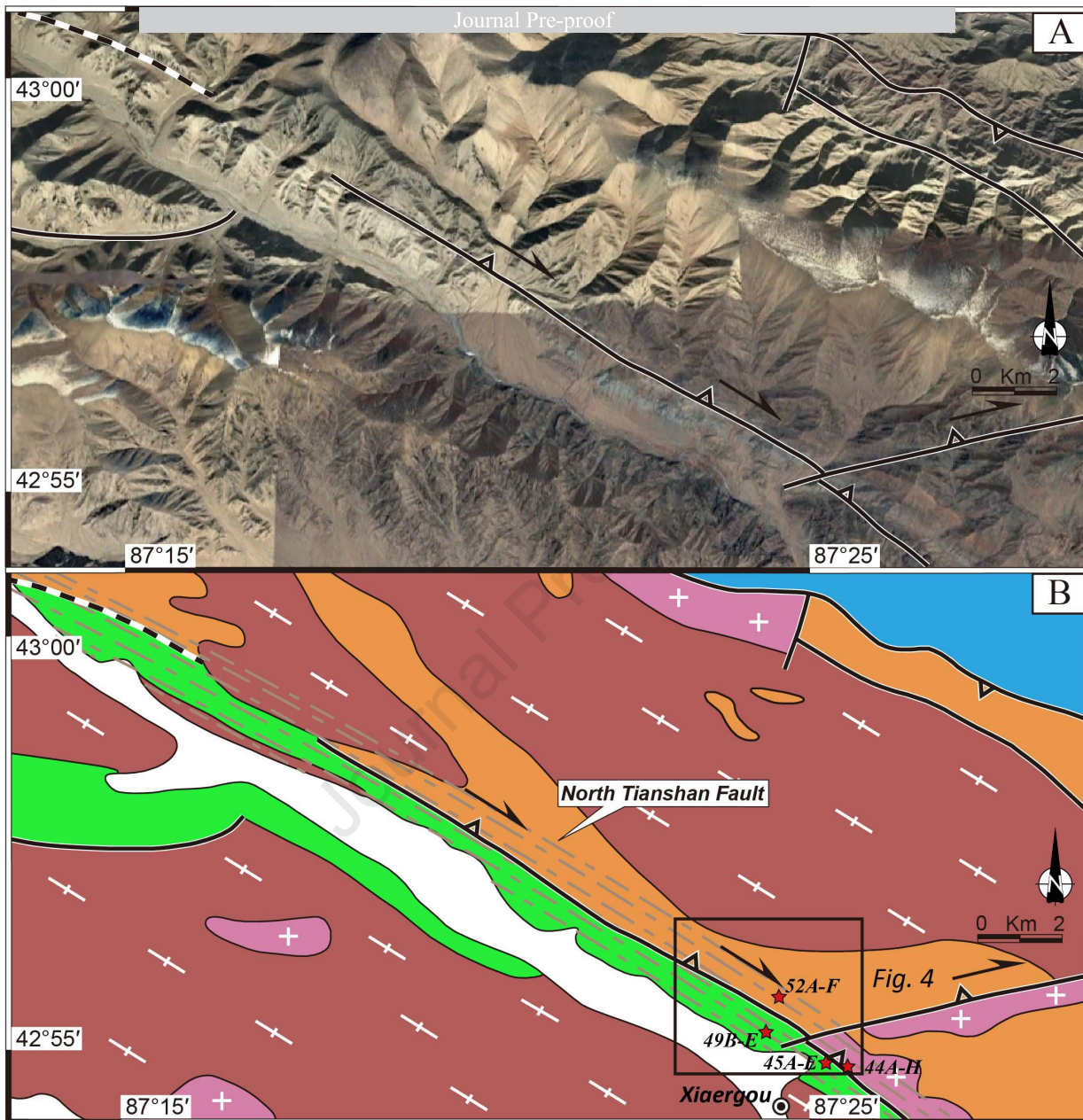
- 1318 Paleo-Asian and Tethyan tectonic systems with docking the Tarim block. *Acta*  
1319 *Petrologica Sinica* 27, 1-22 (in Chinese with English abstract).
- 1320 Yang, T.N., Li, J.Y., Wang, Y., Dang, Y.X., 2009. Late Early Permian (266 Ma) N-S  
1321 compressional deformation of the Turfan basin, NW China: the cause of the  
1322 change in basin pattern. *International Journal of Earth Sciences* 98, 1311-1324.
- 1323 Yang, T.N., Li, J.Y., Wen, Z.T., Feng, X.F., Wang, Y., Sun, G.H., Gao, L.M., 2004.  
1324 Ductile shearing zones occurring along the northern and southern boundaries of  
1325 the central Tianshan block. *Acta Geologica Sinica* 78, 310-320 (in Chinese with  
1326 English abstract).
- 1327 Yang, T.N., Wang, Y., Li, J.Y., Sun, G.H., 2007. Vertical and horizontal strain  
1328 partitioning of the Central Tianshan (NW China): evidence from structures and  
1329  $^{40}\text{Ar}/^{39}\text{Ar}$  geochronology. *Journal of Structural Geology* 29, 1605-1621.
- 1330 Yin, J.Y., Chen, W., Xiao, W.J., Yuan, C., Zhang, B., Cai, K.D., Long, X.P., 2017.  
1331 Geochronology, petrogenesis, and tectonic significance of the latest  
1332 Devonian-early Carboniferous I-type granites in the Central Tianshan, NW China.  
1333 *Gondwana Research* 44, 188-199.
- 1334 Yin, A., Nie, S., 1996. A Phanerozoic palinspastic reconstruction of China and its  
1335 neighboring regions. In: Yin, A., Harrison, T.M. (Eds.), *The Tectonic Evolution*  
1336 *of Asia*. Cambridge University Press, Cambridge, pp. 442-485.
- 1337 Zhang, B., Chai, Z., Yin, C.Y., Huang, W.T., Wang, Y., Zhang, J.J., Wang, X.X., Cao,  
1338 K., 2017. Intra-continental transpression and gneiss doming in an obliquely  
1339 convergent regime in SE Asia. *Journal of Structural Geology* 97, 48-70.
- 1340 Zhang, X.R., Zhao, G.C., Sun, M., Eizenhöfer, P.R., Han, Y.G., Hou, W.Z., Liu, D.X.,  
1341 Wang, B., Liu, Q., Xu, B., 2016. Tectonic evolution from subduction to  
1342 arc-continent collision of the Junggar ocean: constraints from U-Pb dating and  
1343 Hf isotopes of detrital zircons from the North Tianshan belt, NW China.  
1344 *Geological Society of America Bulletin* 128, 644-660.

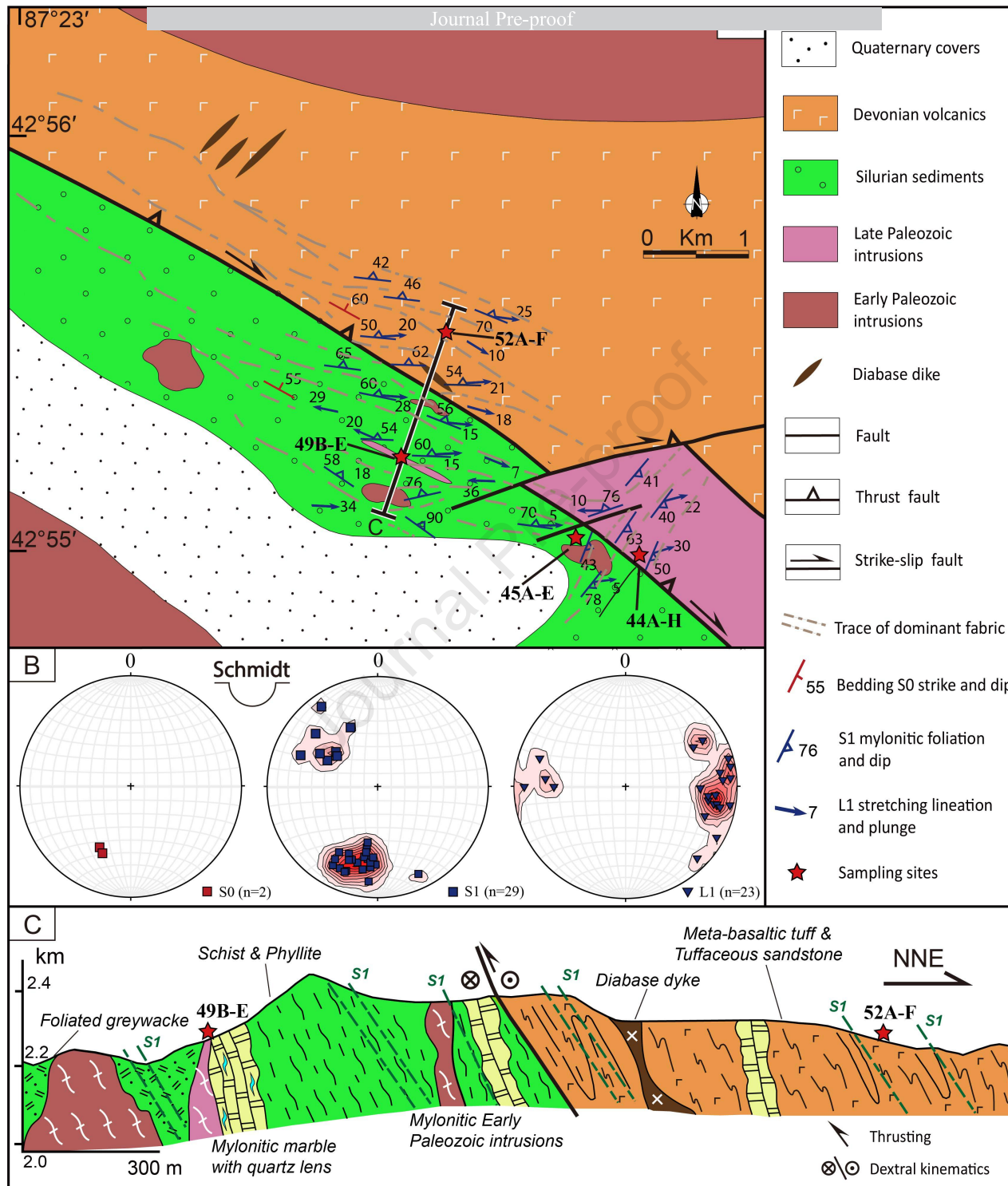
- 1345 Zhong, L.L., Wang, B., Alexeiev, D.V., Cao, Y.C., Biske, Y.S., Liu, H.S., Zhai, Y.Z.,  
1346 Xing, L.Z., 2017. Paleozoic multi-stage accretionary evolution of the SW  
1347 Chinese Tianshan: new constraints from plutonic complex in the Nalati Range.  
1348 *Gondwana Research* 45, 254-274.
- 1349 Zhong, L.L., Wang, B., de Jong, K., Zhai, Y.Z., Liu, H.S., 2019. Deformed continental  
1350 arc sequences in the South Tianshan: New constraints on the Early Paleozoic  
1351 accretionary tectonics of the Central Asian Orogenic Belt 768, (2019) 228169.  
1352 doi.org/10.1016/j.tecto.2019.228169.
- 1353 Zhong, L.L., Wang, B., Shu, L., Liu, H., Mu, L., Ma, Y., Zhai, Y., 2015. Structural  
1354 overprints of early Paleozoic arc-related intrusive rocks in the Chinese Central  
1355 Tianshan: Implications for Paleozoic accretionary tectonics in SW Central Asian  
1356 Orogenic Belts. *Journal of Asian Earth Science* 113, 194-217.
- 1357 Zhou, D., Graham, S.A., Chang, E.Z., Wang, B., Hacker, B., 2001. Paleozoic tectonic  
1358 amalgamation of the Chinese Tian Shan: Evidence from a transect along the  
1359 Dushanzi-Kuqa Highway. In: Hendrix, M.S., Davis, G.A. (Eds.), *Paleozoic and  
1360 Mesozoic Tectonic Evolution of Central Asia: From Continental Assembly to  
1361 Intracontinental Deformation*. Geological Society of America Memoir 194, pp.  
1362 23-46.
- 1363 Zhu, Y.F., 2011. Zircon U-Pb and muscovite  $^{40}\text{Ar}/^{39}\text{Ar}$  geochronology of the  
1364 gold-bearing Tianger mylonitized granite, Xinjiang, northwest China:  
1365 implications for radiometric dating of mylonitized magmatic rocks. *Ore Geology  
1366 Reviews* 40, 108-121.
- 1367 Zhu, X., Wang, B., Chen, Y., Liu, H., 2019b. Constraining the Intracontinental  
1368 Tectonics of the SW Central Asian Orogenic Belt by the Early Permian  
1369 Paleomagnetic Pole for the Turfan-Hami Block. *Journal of Geophysical Research:  
1370 Solid Earth* 124, 12366-12387.
- 1371 Zhu, X., Wang, B., Chen, Y., Liu, H., Horng, C.s., Choulet, F., Faure, M., Shu, L., Xue,

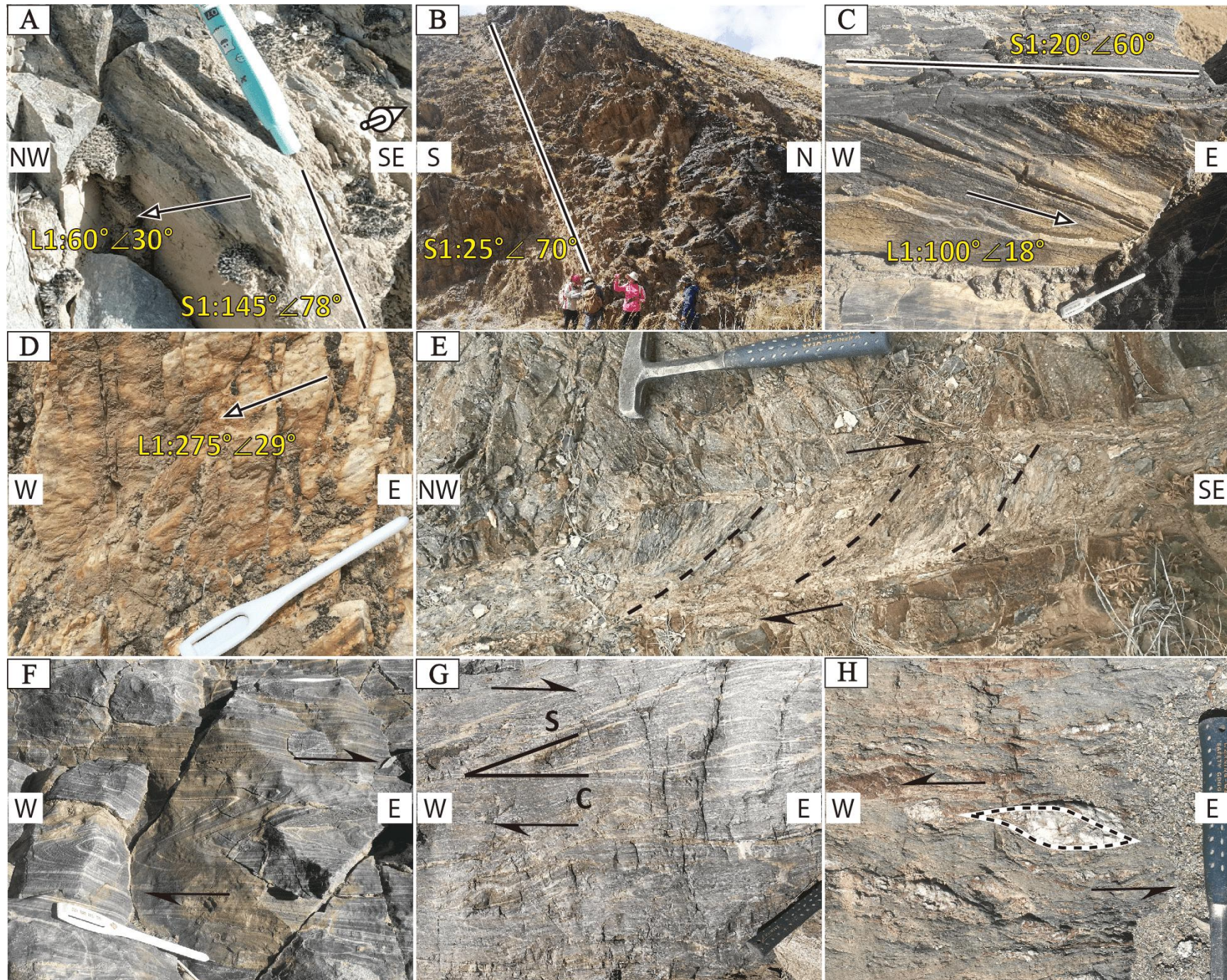
- 1372 Z., 2018. First Early Permian paleomagnetic pole for the Yili Block and its  
1373 implications for Late Paleozoic postorogenic kinematic evolution of the SW  
1374 Central Asian Orogenic Belt. *Tectonics* 37, 1709-1732.
- 1375 Zhu, X.Y., Wang, B., Cluzel, D., He, Z.Y., Zhou, Y., Zhong, L.L., 2019a. Early  
1376 Neoproterozoic gneissic granitoids in the southern Yili Block (NW China):  
1377 constraints on microcontinent provenance and assembly in the SW Central Asian  
1378 Orogenic Belt. *Precambrian Research* 325, 111-131.

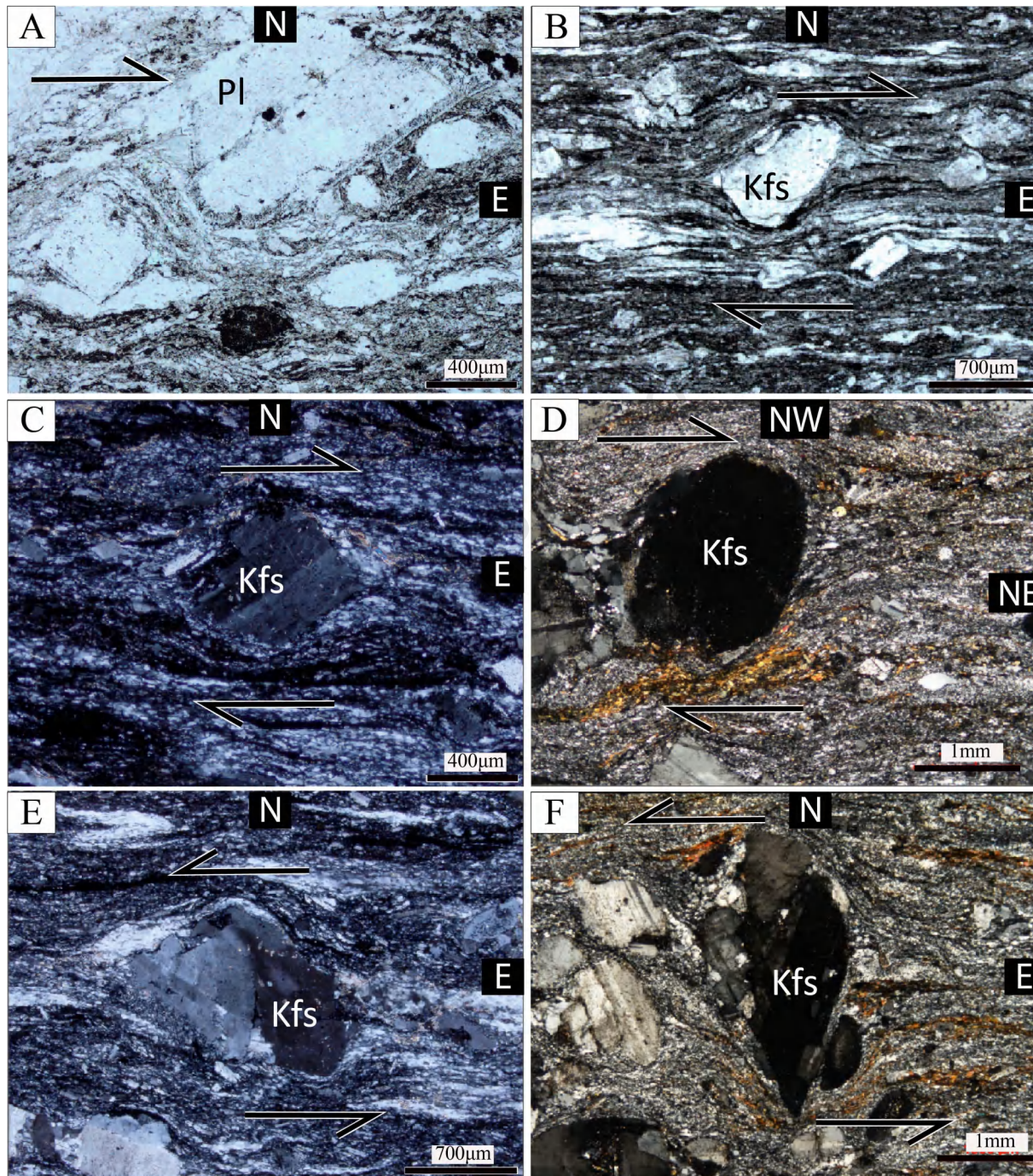


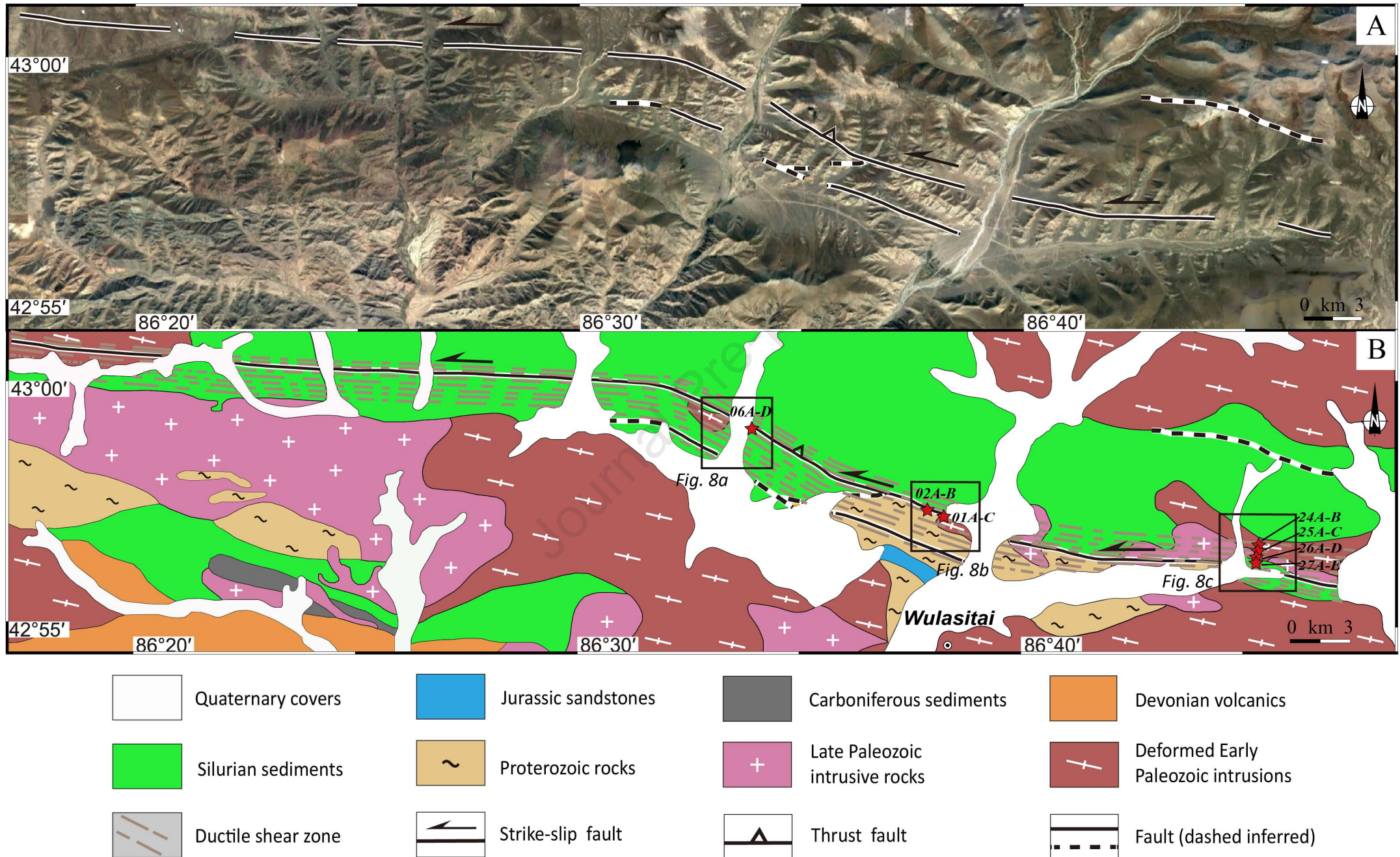




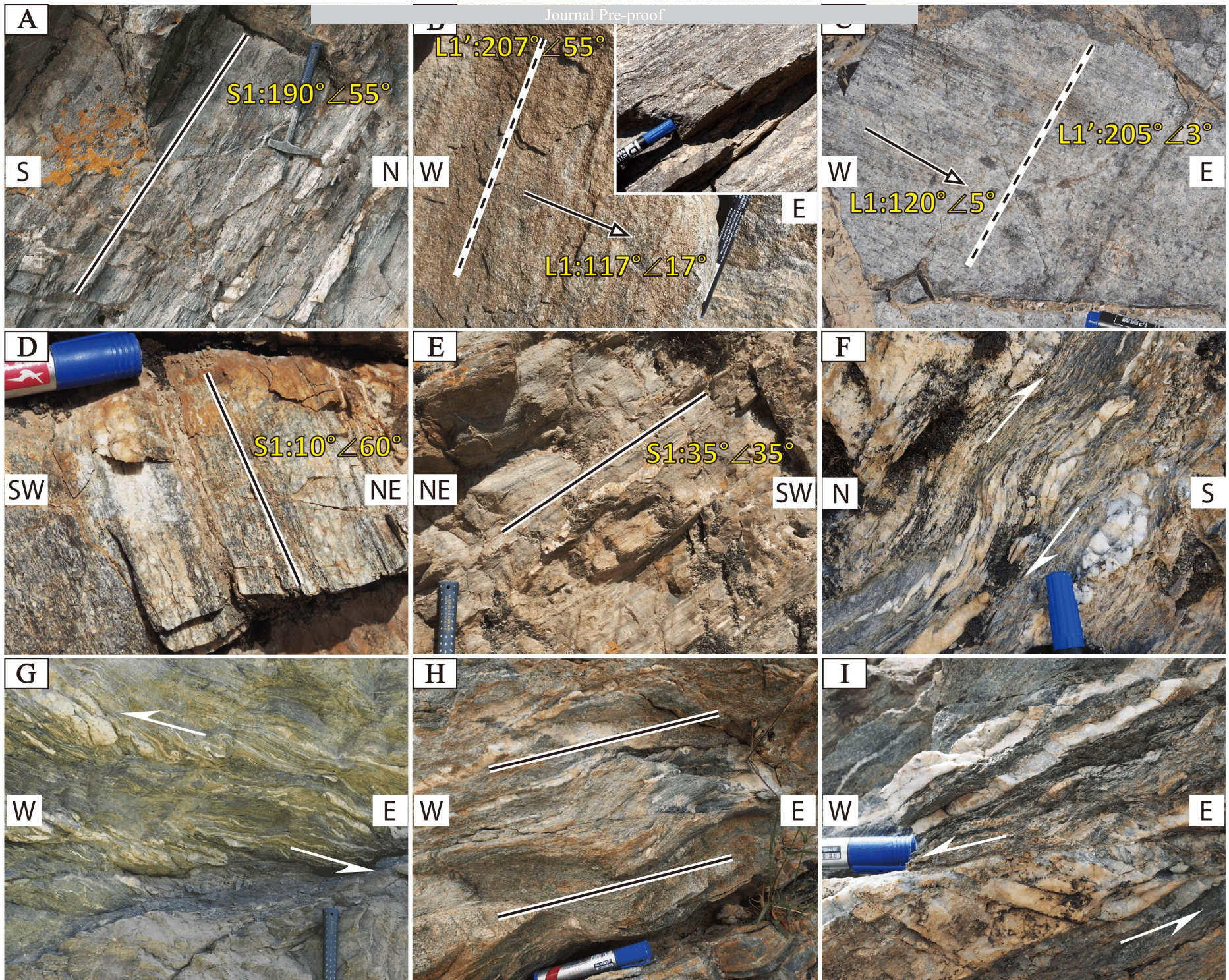


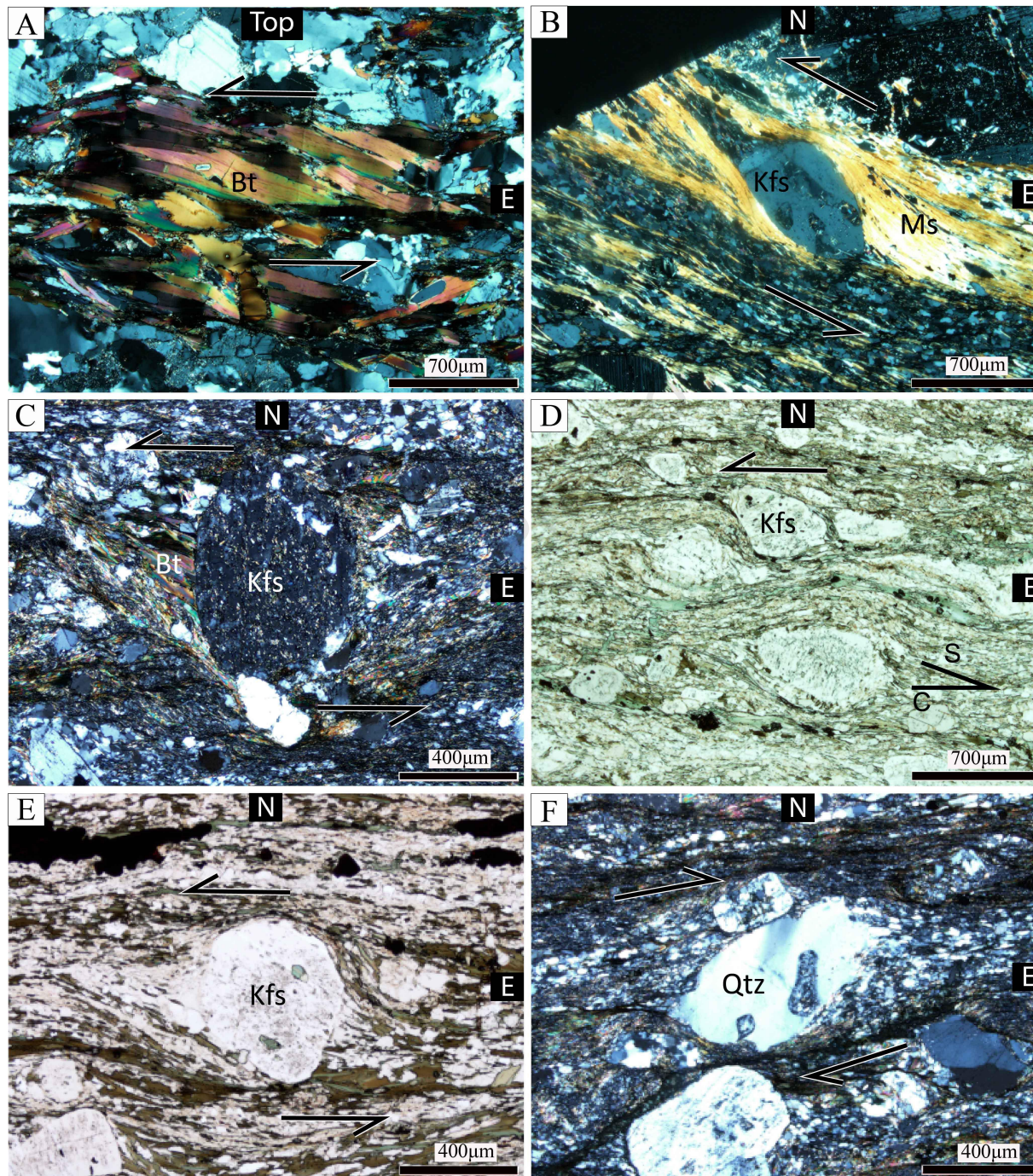


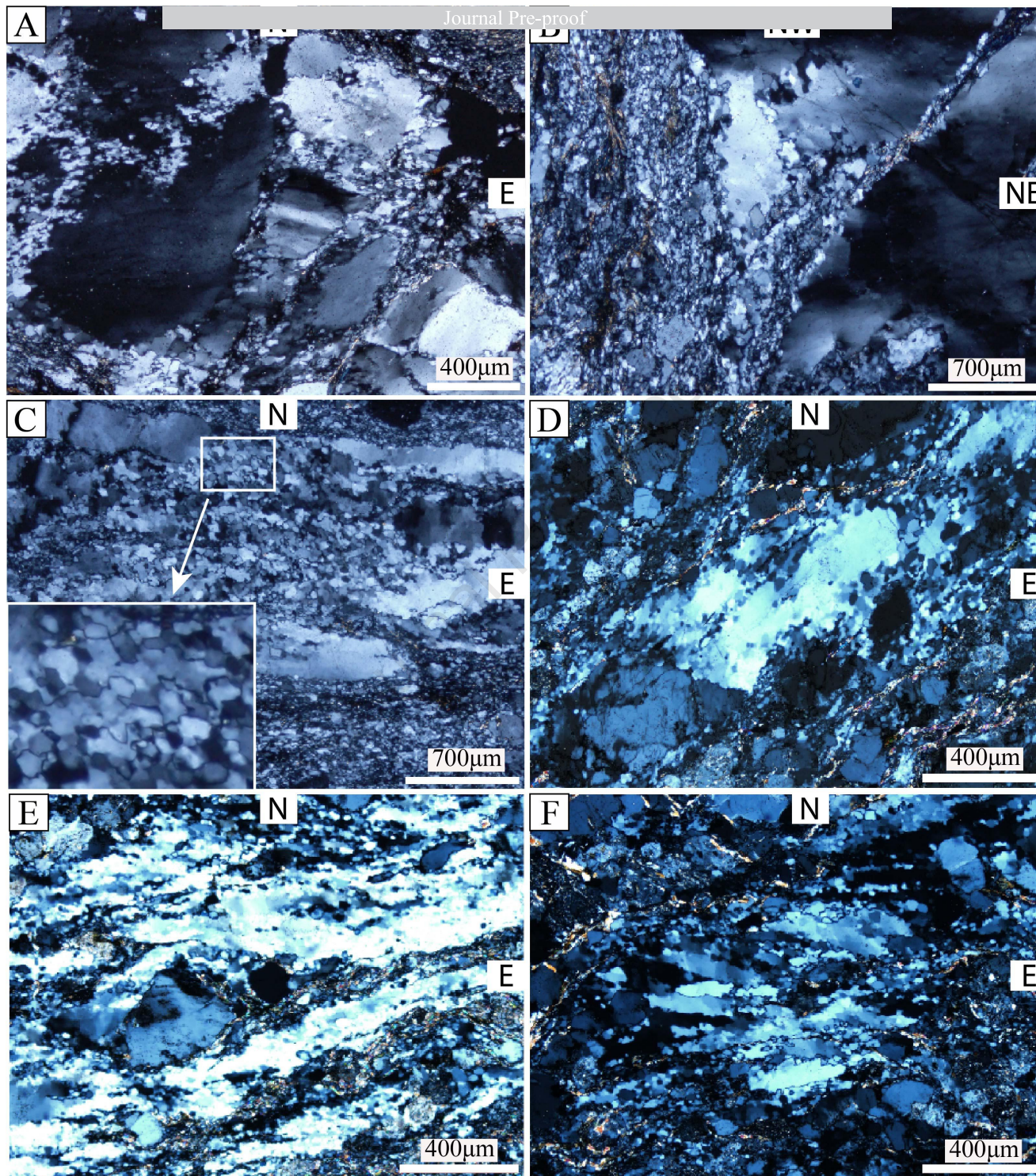


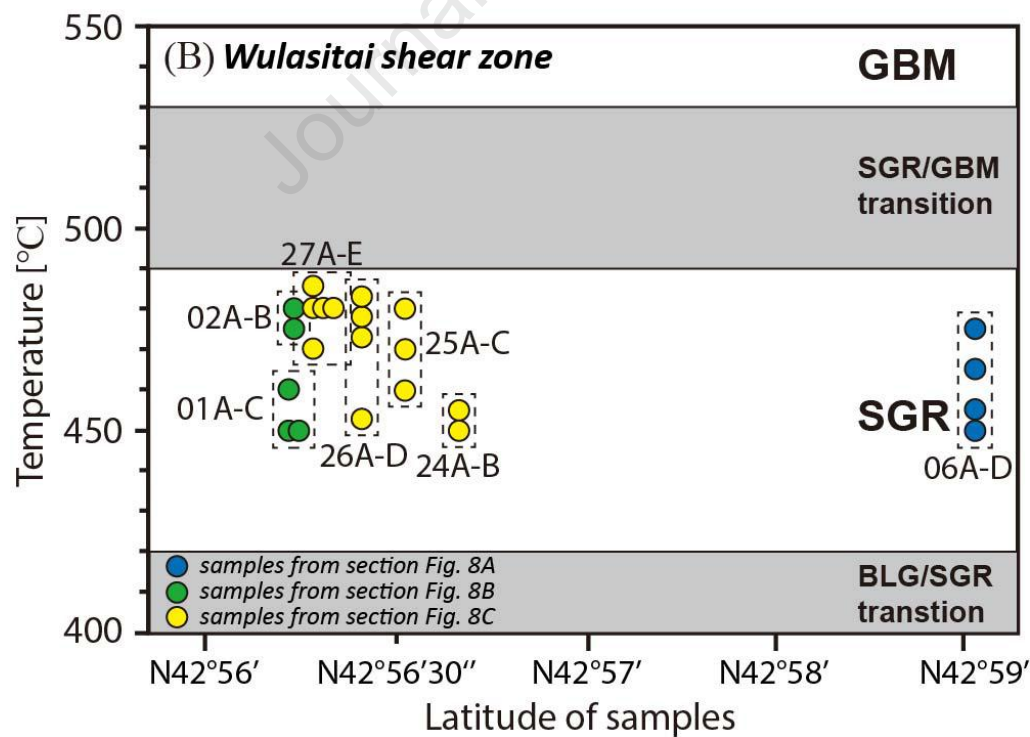
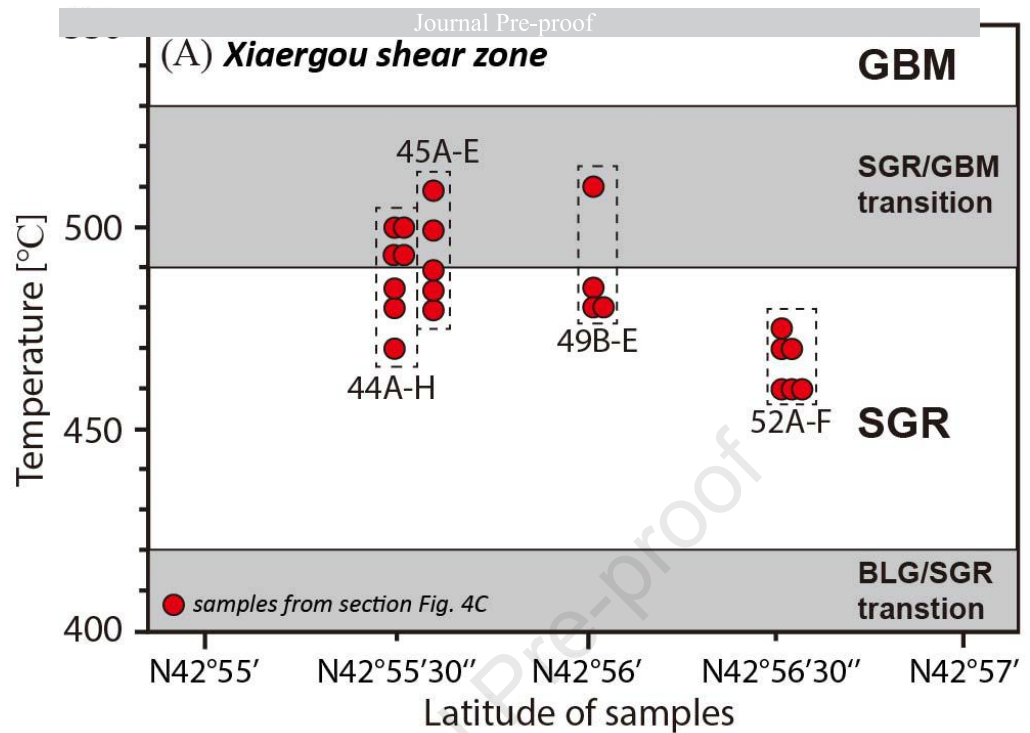


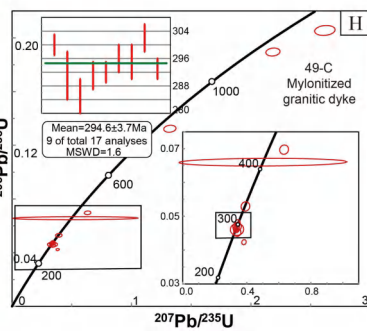
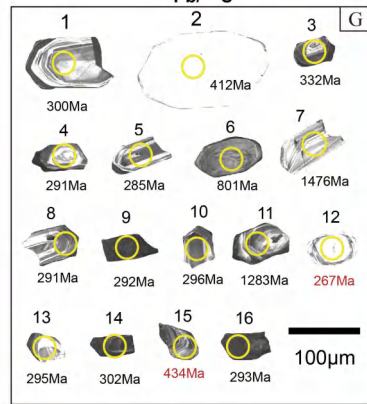
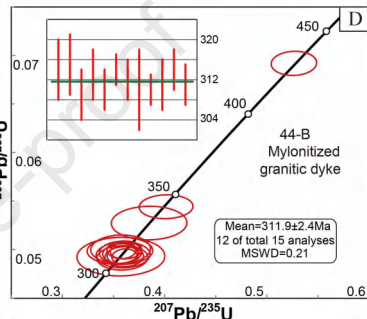
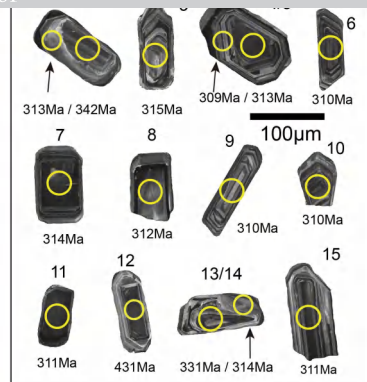
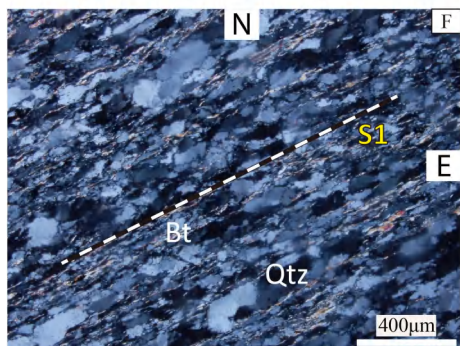
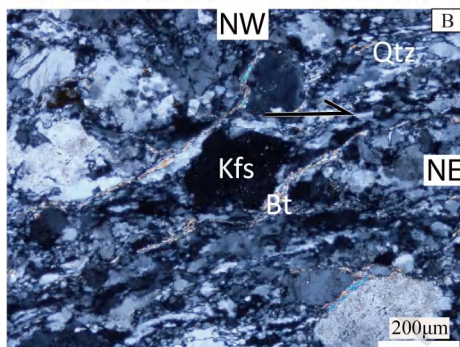


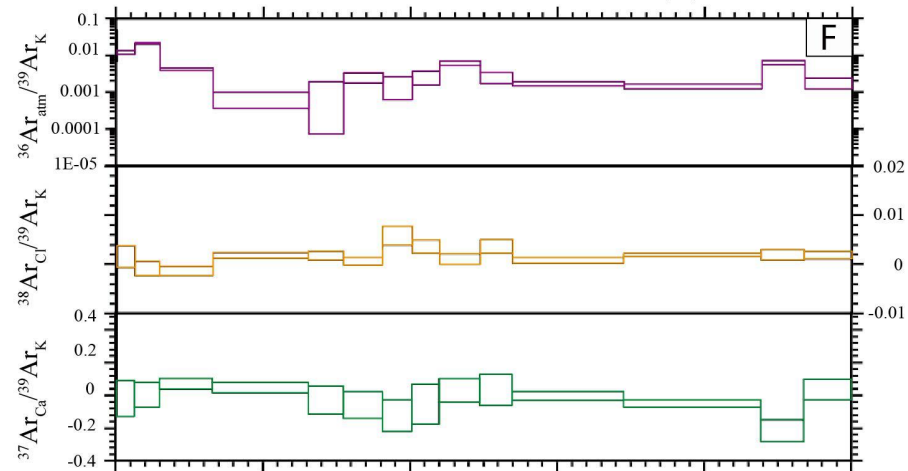
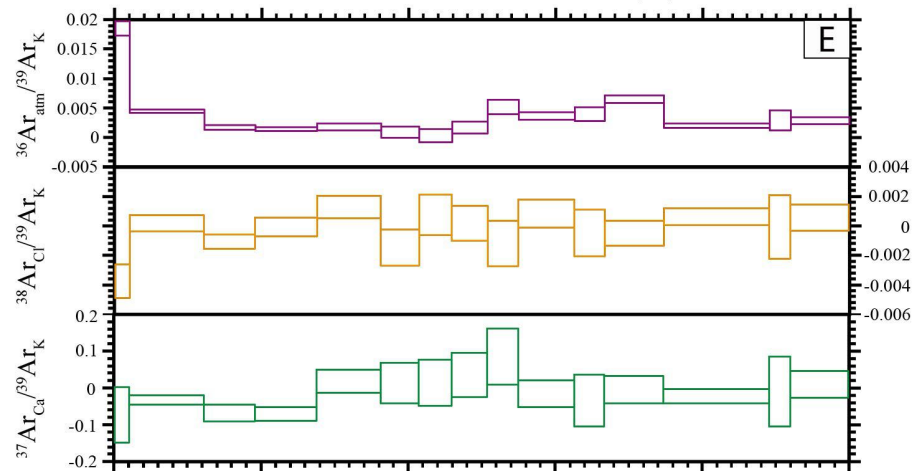
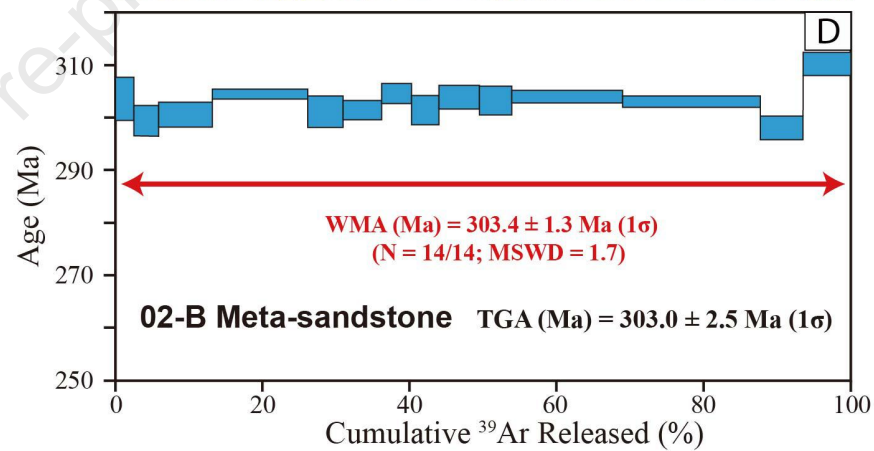
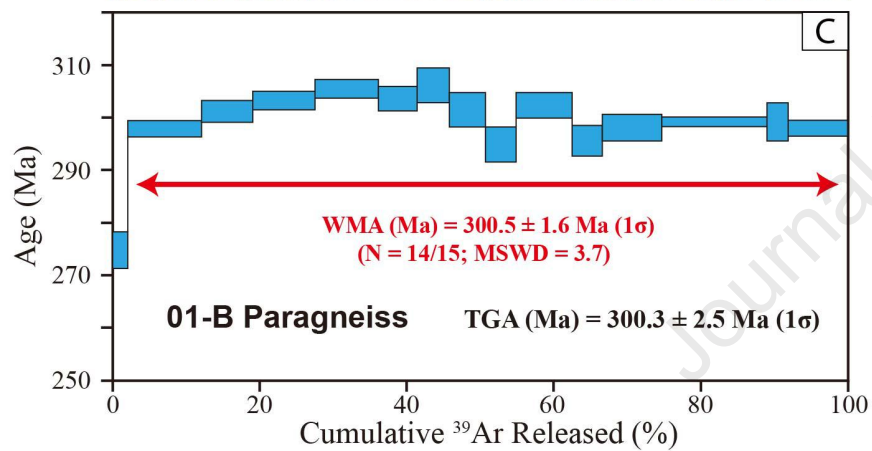
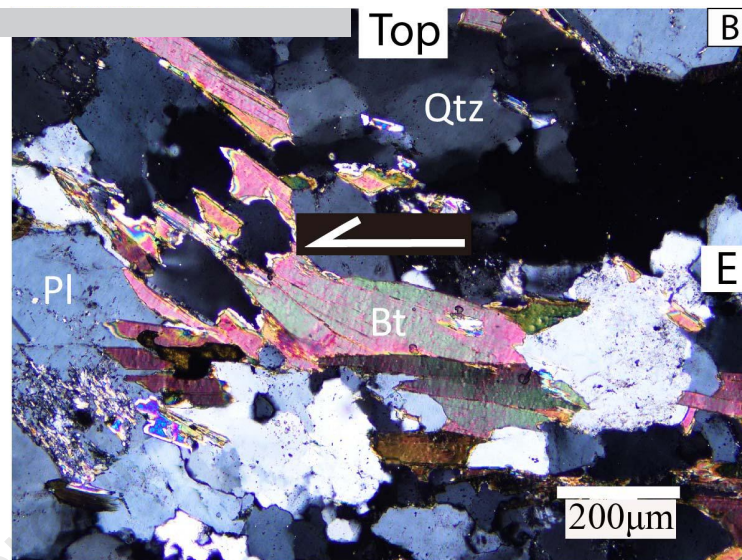
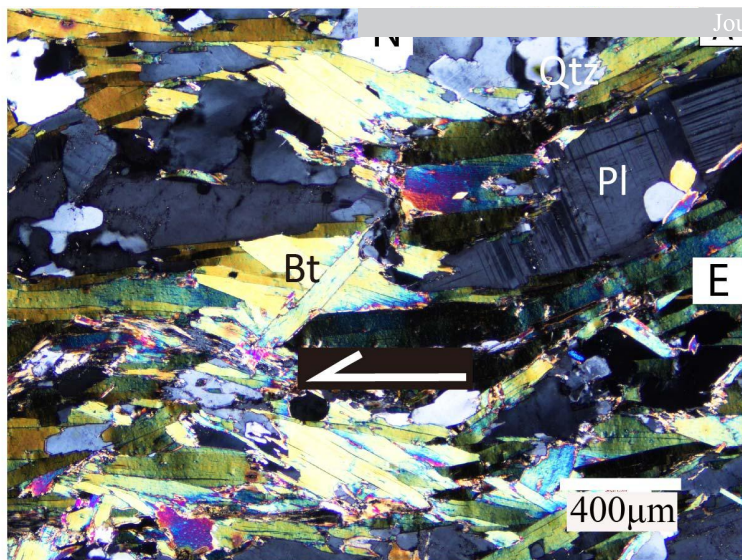




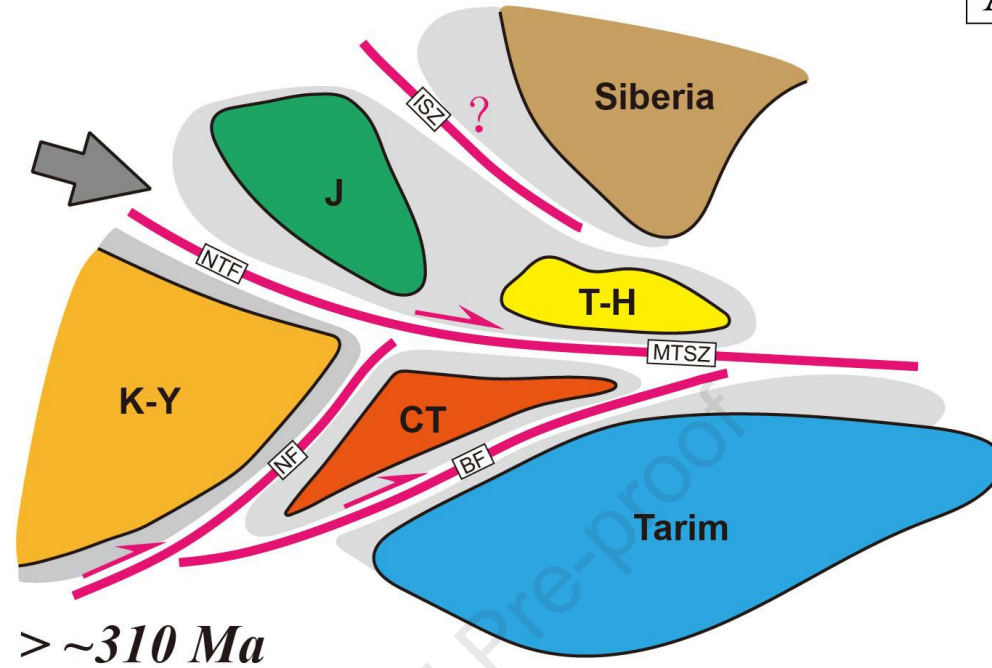




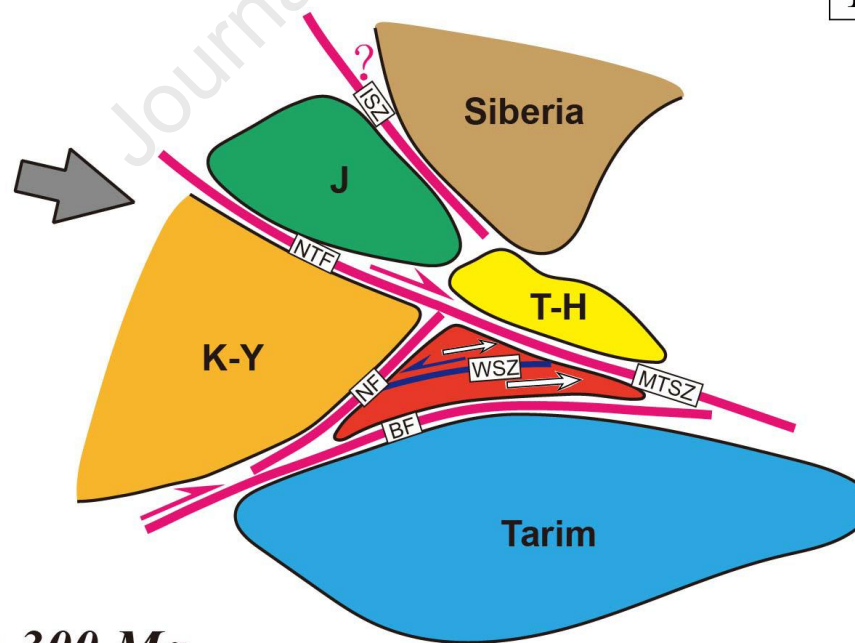




A

 $> \sim 310$  Ma

B

 $\sim 310-300$  Ma

Highlights:

- Xiaergou ductile strike-slip shear zone links the North Tianshan Fault and Main Tianshan Shear zone.
- Wulasitai ductile sinistral strike-slip shear zone occurs inside the Central Tianshan block.
- Ductile strike-slip shear zones around and in Central Tianshan initiated synchronously at ~310 Ma.
- Ductile strike-slip shear zones in SW CAOB denotes its eastward wedging in between Siberia and Tarim.

**Declaration of competing interest**

The authors declare that they are not aware of any competing financial interests or personal relationships that could have appeared to influence the work reported in this paper.

Journal Pre-proof